Reliability Engineering and System Safety 264 (2025) 111303

Contents lists available at ScienceDirect

Reliability Engineering and System Safety

journal homepage: www.elsevier.com/locate/ress

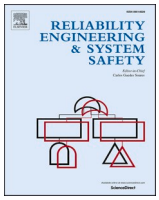

Dynamic inoperability input-output modeling of a system of systems made of multi-state interdependent critical infrastructures

Maria Valentina Clavijo Mesa [a], Francesco Di Maio [a,*], Enrico Zio [b,a]

[a] Energy Department, Politecnico di Milano, Milan, Italy
[b] MINES Paris-PSL University, Centre de Recherche sur les Risques et les Crises (CRC), Sophia Antipolis, France

ARTICLE INFO

Keywords:
Critical infrastructures
System of systems
Interdependencies
Multiple states
Dynamic inoperability input-output model (DIIM)
Network theory
Simulation
Power grid
Water network

ABSTRACT

Critical Infrastructures (CIs) are fundamental for the operation of societies. They function interdependently in a system-of-systems configuration. Interdependencies are unveiled also when CIs become inoperable or only partially operable due to disruptions. The state of partial or full inoperability of a disrupted CI can cascade to the interdependent CIs connected to it in the system of systems, causing various degrees of inoperability. This paper presents a novel approach for modeling the disruption cascade dynamics in multi-state interdependent CIs. A Dynamic Inoperability Input-output Model (DIIM) is proposed to describe the multi-state transition dynamics of the CIs. A case study is worked out to show the application of the proposed approach to a system of systems formed by interdependent power and water networks.

1. Introduction

Critical Infrastructures (CIs) provide essential services to societies, such as power, transportation, telecommunication and healthcare [1]. They are highly interconnected and interdependent on their services for their functioning [2]. However, this also creates ways for disruption in a CI to propagate to other connected ones in the system of systems that they form, with consequent damage to functionality and operability [3]. The terrible event of September 11, 2001, is an example of the offspring of disruptions in interdependent critical sectors, caused by an initiating deliberate attack on one of them [4]. The effects of human error in an offshore oil field in 2010 in the Gulf of Mexico severely impacted the oil and gas industry, devastated marine ecosystems, disrupted tourism and caused significant economic losses in the region [5]. The 2017 Hurricane Harvey in the United States severely disrupted power and communication networks, affecting various industrial and economic activities [6].

Modeling the interdependent functioning of CIs is important to ensure the seamless supply of the essential services they provide to communities [7]. Various approaches have been proposed to quantify the degree of interdependency among CIs [8]. For instance, survey-based approaches quantify interdependencies based on the results of surveys for collecting expert judgment [9]. Limitations to these approaches may come from the difficulty for experts to capture indirect and high-order interdependencies between CIs. Dynamic Bayesian Networks (DBNs) provide a probabilistic framework for modeling interdependencies between CIs [10]. However, expert tuning of DBN parameters make them highly subjective, and their computational cost limits scalability to large-scale systems. Fault Trees can be used to model interdependencies through hierarchical logical relationships [11]. While simple and intuitive, their rigid structure make them unsuitable to capture evolving disruptions and adaptive responses. Also object-oriented approaches can model interdependencies [12,13], but are limited by a static structure not suited to represent the evolving nature of cascading failures and, also, they are quite computationally expensive for large interdependent systems subjected to dynamically evolving disruptions. System dynamic models, on the contrary, can represent interdependencies and time-dependent relationships, offering insights into long-term system evolution [14]. However, their lumped system representations and extensive parameter calibration make them ineffective for real-time disruption management. Data-based approaches leverage real-time CI functional data and mathematical models to analyze interdependencies [15]. These methods aim to incorporate real-time information, offering a more dynamic perspective on CI behavior; however, the small amount of data on dependent effects typically available in practice limits their accuracy [16].

* Corresponding author at: Via Privata Giuseppe La Masa 34, 20156 Milano MI, Italy
E-mail address: francesco.dimaio@polimi.it (F. Di Maio).

https://doi.org/10.1016/j.ress.2025.111303
Received 18 July 2024; Received in revised form 17 March 2025; Accepted 29 May 2025
Available online 30 May 2025

Nomenclature

M	Set of interdependent CIs
$\overline{q}$	Inoperability vector
q_i	Inoperability value of the i-th CI
$\overline{\overline{A}}$	Interdependency matrix
$\overline{\overline{A}}(t+1)$	Multi-state interdependency matrix
a_{ij}	Interdependency coefficient representing the inoperability induced on the i-th infrastructure by the inoperability of the j-th infrastructure
a_{ji}	Interdependency coefficient representing the inoperability induced on the j-th infrastructure by the inoperability of the i-th infrastructure
$\overline{c}$	Perturbation vector
c_i	Inoperability of the i-th CI due to direct effects of an external perturbation
$\overline{\overline{K}}$	Recovery matrix
k_{ii}	Recovery rate coefficient for the i-th CI
G^i	Directed graph of the i-th CI
N^i	Set of nodes in the i-th CI
n_z^i	z-th node of the i-th CI
$E^{(i,i)}$	Set of edges in the i-th CI
$e_{op}^{(i,i)}$	Direct connection from node n_o^i to n_p^i in the i-th CI
$K_{n_z^i}$	Number of states of node n_z^i in the i-th CI
$\overline{x}^{n_z^i}$	State variable vector of node n_z^i in the i-th CI
X_l^i	State l of the i-th CI
$\overline{X}^i$	State variable vector of the i-th CI
$O(X_l^i)$	Operational performance of the i-th CI in state X_l^i
$D(X_l^i)$	Demand met by the i-th CI in state X_l^i
$i \leftrightarrow j$	Interdependency between the i-th and the j-th CIs
$i \rightarrow j$	Dependency of the j-th CI on the i-th CI
$j \rightarrow i$	Dependency of the i-th CI on the j-th CI
$N_{i\rightarrow j}^i$	Set of nodes in the i-th CI responsible for the dependency of the j-th CI on the i-th CI
$N_{i\rightarrow j}^j$	Set of nodes in the j-th CI responsible for the dependency of the j-th CI on the i-th CI
$N_{j\rightarrow i}^i$	Set of nodes in the i-th CI responsible for the dependency of the i-th CI on the j-th CI
$N_{j\rightarrow i}^j$	Set of nodes in the j-th CI responsible for the dependency of the i-th CI on the j-th CI
$E^{(i,j)}$	Set of edges from the i-th CI to the j-th CI
$E^{(j,i)}$	Set of edges from the j-th CI to the i-th CI
$S_{i\rightarrow j}^i$	Set of states of nodes in $N_{i\rightarrow j}^i$
$S_{i\rightarrow j}^j$	Set of states of nodes in $N_{i\rightarrow j}^j$
$S_{j\rightarrow i}^i$	Set of states of nodes in $N_{j\rightarrow i}^i$
$S_{j\rightarrow i}^j$	Set of states of nodes in $N_{j\rightarrow i}^j$
$\overline{\overline{M}}_{i\rightarrow j}$	Dependency matrix related to the dependency $i \rightarrow j$
$\overline{\overline{M}}_{j\rightarrow i}$	Dependency matrix related to the dependency $j \rightarrow i$
r^i	Number of intervals in which the inoperability domain of the i-th CI is discretized
r_e^i	Inoperability interval e of r^i
$a_{ji}(r_e^i)$	Interdependency coefficient representing the inoperability induced on the j-th infrastructure when the inoperability of the i-th infrastructure is in the range r_e^i of inoperability
$\overline{\overline{R}}_{i\rightarrow j}$	Conditional probability matrix related to the dependency $i \rightarrow j$
$\overline{\overline{R}}_{j\rightarrow i}$	Conditional probability matrix related to the dependency $j \rightarrow i$
$\overline{\overline{A}}_i$	Interdependency coefficient matrix for the i-th CI
$\overline{\overline{A}}_j$	Interdependency coefficient matrix for the j-th CI
T	Number of Monte Carlo simulations Abbreviation
CI	Critical infrastructure
DIIM	Dynamic Inoperability Input-output Model
IIM	Inoperability Input-output Model
MW	Megawatt

The Inoperability Input-Output Model (IIM) offers a mathematical framework suitable for catching high-order interdependencies (i.e., indirect relationships between CIs) [17]. However, at the expense of losing details on the subsystems and components constituting each CI, IIM models each CI as an individual entity and captures the interdependencies at such a macroscopic level [18]. The Dynamic Inoperability Input-Output Model (DIIM) [19] is an extension of the IIM that incorporates a temporal dimension to consider the dynamics of the processes (e.g. disruption cascade and recovery) occurring in the system of systems of interconnected CIs. DIIM has proven effective in analyses of interdependent systems, including for example the disruption of several CIs in Italy [20], the impact of COVID-19 on some CIs [21] or that of the Taal volcano eruption in the Philippines in January 2020 [22].

In DIIM, interdependencies are represented by a deterministic and time-invariant interdependency matrix [23]. To introduce flexibility, some studies propose interval arithmetic to account for coefficient uncertainty [24] or expert-driven adjustments for time-varying interdependencies [25]. However, these methods are constrained by the assumption of time-invariant Boolean states, that does not allow to describe changes in the interdependencies during the evolving disruption, as it occurs in real-world scenarios. Studies such as [25] have shown that interdependency coefficients can increase as disruption persist over time, reinforcing the idea that fixed coefficients do not fully represent the effects of the cascading process in real-world scenarios. On the other hand, it is the change in CI states due to the disruption evolution or its recovery that impact on the interdependencies, and whereas [25] models increasing interdependencies as a function of time, it still assumes Boolean infrastructure states, whereas CIs can experience varying degrees of inoperability, which affect interconnected systems differently. This can be captured by considering a multi-state representation for the interdependent infrastructures.

This paper proposes a hybrid DIIM-network theory framework for: introducing a multi-state DIIM framework to represent the varying operational conditions in the system of systems of CIs for the dynamic assessment of disruption evolution; developing a procedure for the estimation of the interdependency coefficients that considers both CI topology and CI physical behavior, reducing reliance on subjective expert assumptions. This is obtained by: i) network theory to delineate the structure and operational characteristics of each CI, and ii) stochastic scenario exploration to systematically map interdependencies based on the inoperability states of subsystems and components.

The integration of the DIIM formulation with network theory allows the identification of critical nodes, to be targeted for protection and mitigation, and improves computational efficiency for large-scale infrastructure networks.

The remainder of the paper is organized as follows. Section 2 describes the DIIM. Section 3 outlines the novel approach for modeling the multi-state CIs and their interdependencies. Section 4 presents a case study regarding interconnected power and water networks, wherein

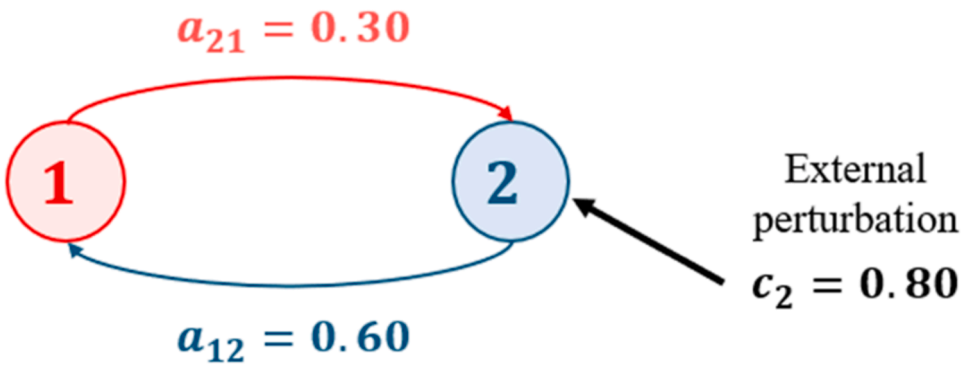

Fig. 1. Example of interdependent CIs.

each CI has five possible operational states, each one differently affecting the response of the interdependent CIs upon disruption and, thus, ultimately affecting the operability of the system of systems made by the interconnected CIs. Section 5 discusses the results and compares them with those of a traditional DIIM approach, and the use of multi-state DIIM for the identification of the most critical nodes and the adoption of mitigation strategies. Finally, Section 6 presents some conclusions and reflections on directions for future research.

2. Overview of DIIM

The fundamental equation of IIM is [19]:

$$\overline{q} = \overline{\overline{A}}\overline{q} + \overline{c} = [\overline{\overline{I}} - \overline{\overline{A}}]^{-1}\overline{c} \tag{1}$$

where $\overline{q}$ is the vector of inoperability values $q_i,\ i = 1, \ldots, M$, of the M interconnected CIs, indicating the proportion of the total planned production/service that remains unrealized/unsupplied due to disruptions [26]. The values of q_i range from 0 (fully operational, meaning the production is completely realized) to 1 (fully inoperable, where no planned production is realized) [27]. $\overline{\overline{A}}$ is a $M \times M$ matrix whose entry a_{ij} is the interdependency coefficient that governs the inoperability induced by the j-th infrastructure on the i-th infrastructure when the j-th infrastructure is in a completely inoperable state ($q_j = 1$); $\overline{c}$ is the perturbation vector, whose entry c_i is the inoperability of the i-th CI due to direct effects of external perturbations, such as accidental events, natural disasters and targeted attacks, which cause disruptions [18].

For example, considering the system of systems illustrated in Fig. 1, which shows two interdependent CIs, where the complete inoperability of infrastructure 1 ($q_1 = 1$) leads to a 30 % inoperability of infrastructure 2 and the complete inoperability of infrastructure 2 ($q_2 = 1$) leads to a 60 % inoperability of infrastructure 1, the $\overline{\overline{A}}$ matrix is:

$$\overline{\overline{A}} = \begin{pmatrix} 0 & 0.6 \\ 0.3 & 0 \end{pmatrix} \tag{2}$$

If an external perturbation occurs and disrupts the operation of infrastructure 2 to a state of 80 % inoperable, the overall inoperabilities of the interdependent infrastructures 1 and 2 in the system of systems are calculated as follows, from Eq. (1):

$$\begin{pmatrix} q_1 \\ q_2 \end{pmatrix} = \begin{pmatrix} 0 & 0.6 \\ 0.3 & 0 \end{pmatrix}\begin{pmatrix} q_1 \\ q_2 \end{pmatrix} + \begin{pmatrix} 0 \\ 0.8 \end{pmatrix} = \begin{pmatrix} 0.6q_2 \\ 0.3q_1 + 0.8 \end{pmatrix} = \begin{pmatrix} 0.59 \\ 0.98 \end{pmatrix} \tag{3}$$

Although IIM allows accounting for the interdependency between CIs and its effects on their inoperability, it misses: i) a dynamic perspective for modeling the disruption evolution and the system-of-systems recovery process in time, ii) a detailed description of the state of each CI, beyond the Boolean dichotomy of fully operable and fully inoperable ($q = 0$ or $q = 1$), to describe the interdependency (and estimate the related coefficients).

To overcome the first limitation, DIIM was introduced as an extension of the traditional IIM [28], to model the dynamics of the behavior of interdependent CIs in relation to their inoperability states upon the occurrence of disruptions that affect their operation. The fundamental equation of DIIM (considering discrete time steps of one arbitrary unit of time) is [29]:

$$\overline{q}(t+1) = \overline{q}(t) - \overline{\overline{K}}\overline{q}(t) + \overline{\overline{K}}\overline{\overline{A}}\overline{q}(t) + \overline{\overline{K}}\overline{c}(t) \tag{4}$$

The time-dependent description of the system-of-systems inoperability upon disruption is obtained by considering that the inoperability vector at time $t+1$, $\overline{q}(t+1)$, is:

- the inoperability vector at time t, $\overline{q}(t)$;
- minus the inoperability recovery achieved through the inherent recovery capabilities of each CI in the system of systems, modeled by the diagonal $M \times M$ matrix $\overline{\overline{K}}$ where each entry k_{ii} represents the recovery rate coefficient of the i-th CI, i.e. the speed at which each CI can recover from inoperability [29,30];
- plus the term $\overline{\overline{K}}\overline{\overline{A}}\overline{q}(t)$, which accounts for the propagation of inoperability across the CIs of the system of systems through their interdependencies at time t, modulated by their respective recovery rates;
- plus the increase in inoperability that occurs at the next time step $t+1$ due to external perturbations, $\overline{\overline{K}}\overline{c}(t)$, also adjusted by the ability of each CI to recover from its perturbations.

As built, Eq. (4) provides a model to describe the dynamic interactions and external influences affecting the inoperability of interconnected CIs in a system-of-systems context. The values of the recovery matrix $\overline{\overline{K}}$ are estimated based on CI-specific recovery data, accounting for factors such as historical restoration times, infrastructure redundancy, and operational or location constraints. Larger recovery coefficients correspond to faster system recovery, as discussed by [31]. The reader may refer to [3,29] and [32] for methodologies to estimate these coefficients.

Considering the previous case of the two CIs with $\overline{\overline{A}}$ as in Eq. (2), the initial inoperability conditions calculated as estimated in Eq. (3) and the following recovery matrix:

$$\overline{\overline{K}} = \begin{pmatrix} \frac{1}{14(1-a_{11})} ln\left(\frac{1}{0.01}\right) & 0 \\ 0 & \frac{1}{21(1-a_{22})} ln\left(\frac{1}{0.01}\right) \end{pmatrix} = \begin{pmatrix} 0.33 & 0 \\ 0 & 0.22 \end{pmatrix} \tag{5}$$

Those recovery values are estimated from the typical restoration times of each CI, (i.e., 14 and 21 days for infrastructures 1 and 2,

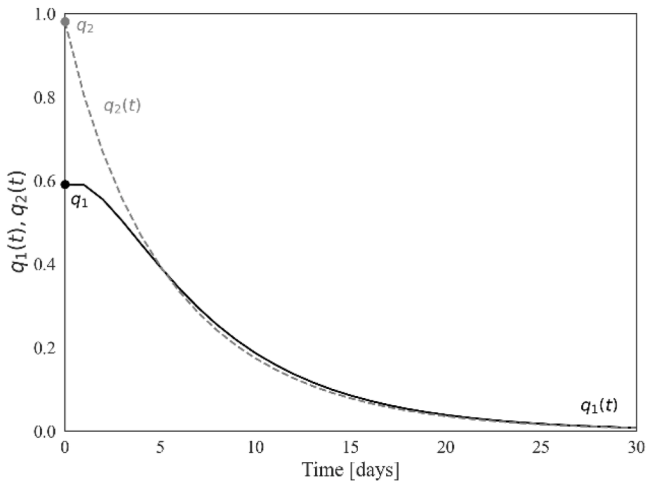

Fig. 2. Inoperability of infrastructure 1 (continuous line) and infrastructure 2 (dashed line).

respectively as in [33]).

We can provide the evolution of the inoperability q_1 and q_2 over discrete time steps, using Eq. (6):

$$\begin{aligned} q_1(t+1) &= q_1(t) - 0.33q_1(t) + 0.20q_2(t) + 0.33c_1(t) \\ q_2(t+1) &= q_2(t) - 0.22q_2(t) + 0.07q_1(t) + 0.22c_2(t) \end{aligned} \tag{6}$$

The resulting time-dependent inoperability curves q_1 and q_2 are those shown in Fig. 2.

Still, like IIM, the DIIM assumes Boolean states for the CIs when defining the degree of interdependency between infrastructures, which is not necessarily realistic. To address this limitation, in the next Section, we propose a novel approach to extend the DIIM for modeling multi-state interdependent CIs.

3. Modeling multi-state interdependent CIs

CIs can either be dependent or interdependent. Dependencies involve unidirectional influences, whereas interdependencies involve bidirectional relationships where the states of the CIs mutually influence each other [34]. In the DIIM, dependencies and interdependencies are modeled using the interdependency matrix ($\overline{\overline{A}}$). However, this is done neglecting the internal structure of the CIs with their subsystems and components, which can be in multiple states and have various degrees of dependence. This could lead to wrong estimation of the actual damage state of the CIs following a cascading failure process through the dependencies and interdependencies, as highlighted in [35]. Indeed, dependencies and interdependencies of various degrees exist between the subsystems and components of the CIs. This can lead to different cascading failure scenarios through the dynamic propagation of a disruption.

To account for the internal characteristics of the CIs, the interdependency coefficients should reflect these relationships and the multiple states of inoperability that emerge from the cascading processes. To this aim, the inoperability domain ([0,1]) of each CI is discretized into ranges of increasing inoperability and for each range r^j of the j-th CI, an interdependency coefficient $a_{ij}(r^j)$ is estimated (and correspondingly, for each range r^i of the i-th CI influencing the j-th CI, i.e., $a_{ji}(r^i)$).

For example, let us consider a system of systems of interdependent CIs composed of a power grid (CI i) and a telecommunication network (CI j), whose interdependency is shown in Fig. 3. The inoperability states of both CIs i and j are grouped into two ranges r_1^i, r_2^i and r_1^j, r_2^j of small and large inoperability, respectively. When the power grid experiences minor inoperability ($q_i \in r_1^i$), the functionality of the telecommunication network could be reduced, e.g., by resorting to backup power units, which would thus be characterized by a small value of the interdependency coefficient $a_{ji}(r_1^i)$, whereas a complete power grid blackout ($q_i = 1 \in r_2^i$) could cause the telecommunication network to be completely inoperable, which would correspond to a large value of the interdependency coefficient $a_{ji}(r_2^i)$. Conversely, the power grid relies on telecommunication for monitoring and control tasks: a minor inoperability of the telecommunication network ($q_j \in r_1^j$), would be corresponding to a small interdependency coefficient $a_{ij}\left(r_1^j\right)$, whereas an inoperable telecommunication network ($q_j = 1 \in r_2^j$) would expose the power grid to large-scale outages, and in this case interdependency is described by a large value of interdependency coefficient $a_{ij}\left(r_2^j\right)$. In other words, the

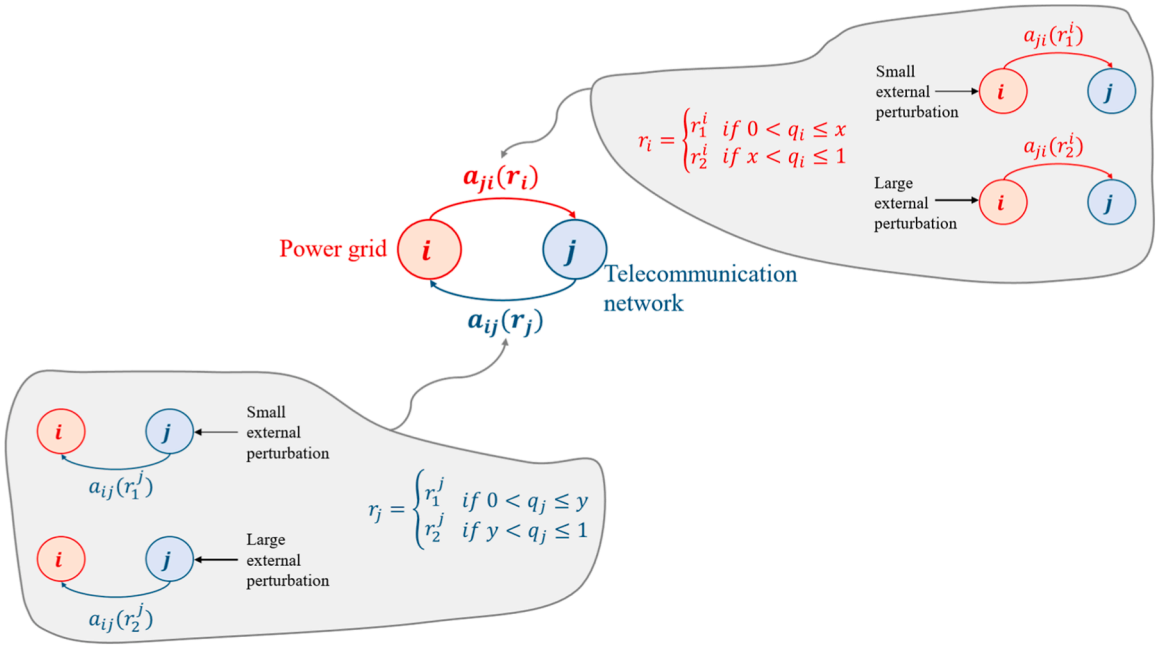

Fig. 3. Example of interdependency coefficients in multi-state interdependent CIs: power grid (CI ***i***) and telecommunication network (CI ***j***).

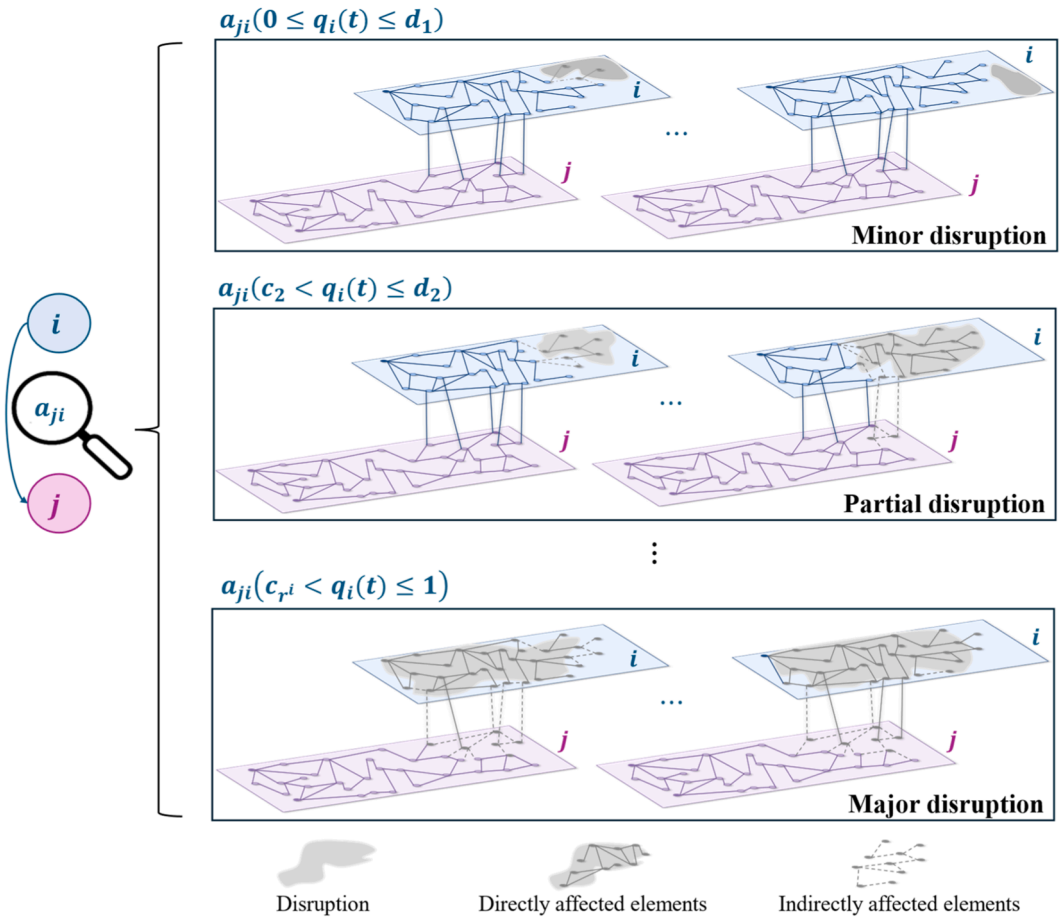

Fig. 4. Multi-state interdependency for the hypothetical example of two CIs, ***i*** and ***j***.

interdependency varies with the inoperability levels of the involved interdependent CIs and a novel approach is needed for interdependency coefficients estimation, realistically modeling interdependencies between multi-state CIs, as also argued in [36].

3.1. Extending the interdependency matrix to multi-state CIs

To represent the interdependence of multi-state CIs, a multi-state interdependency matrix $\overline{\overline{A}}(t+1)$ of multi-state interdependency coefficients is introduced and updated based on the inoperability values of the CIs at each time t. This allows us to retain the high-level interdependency matrix of the traditional DIIM, while incorporating detailed information from the internal states of the CIs subsystems/components and their dynamic interactions within the system of systems.

Fig. 4 illustrates the conceptualization of the modeling of the multi-state dependency of a hypothetical j-th CI on a hypothetical i-th CI, and the evolution of the interdependency coefficients as a function of inoperability intervals, where the interdependency coefficient a_{ji} takes different values depending on the inoperability state of the i-th CI (at time t). For this, the inoperability range $[0, 1]$ for the i-th CI is partitioned into a set of intervals $r_e^i = \{[c_e, d_e]\}$ for $e = 1, \ldots, r^i$, where $0 = c_1 < d_1 = c_2 < d_2 = \ldots = c_{r^i} < d_{r^i} = 1$; then, at any given time t, the value of the coefficient a_{ji} is determined by the inoperability value $q_i(t)$. In other words, a_{ji} depends on the interval r^i in which $q_i(t)$ falls.

In real-world applications, the range of validity of the a_{ji} for each inoperability state is to be determined based on empirical data or/and by expert judgment.

To detail the modeling framework proposed in this paper, the extension of the traditional interdependency matrix to a multi-state involves three phases:

(1) Characterization of the multi-state CIs using network theory;
(2) Mapping of the interdependencies between the multi-state CIs;
(3) Estimation of the interdependency coefficients by simulation.

3.2. Characterization of the multi-state CIs

The first phase involves describing the operational and topological characteristics of each CI of the system of systems considered.

The topological structure of each CI can be defined using network theory [37,38]. Specifically, each generic i-th CI ($i = 1, \ldots, M$) is represented as a directed graph $G^i \equiv (N^i, E^{(i,i)})$, where $N^i = \{n_1^i, n_2^i, \ldots, n_Z^i\}$ are the Z nodes (subsystems or component groups) of the i-th CI network, and $E^{(i,i)} = \left\{e_{op}^{(i,i)} = \left(n_o^i, n_p^i\right) \subseteq N^i \times N^i\right\}$ is the set of edges $e_{op}^{(i,i)}$ connecting the nodes n_o^i and n_p^i of the i-th CI, G^i [39].

To consider the multiplicity of states, it is necessary to introduce the $K_{n_z^i}$ states for each generic z-th node n_z^i, ($z = 1, \ldots, Z$), and the state variable vector $\overline{x}^{n_z^i} = \left[x_1^{n_z^i}, x_2^{n_z^i}, \ldots, x_{K_{n_z^i}}^{n_z^i}\right]$, where the variable $x_1^{n_z^i}$ corresponds to the perfect functioning state of the generic node n_z^i and $x_{K_{n_z^i}}^{n_z^i}$ represents the complete failure state of the generic node n_z^i. The states of the nodes are mutually exclusive, that is, if the node is in one of its possible states, it cannot simultaneously be in another one and correspondingly the state variables are binary, taking the value 1 if the node is in the respective state and 0 otherwise [40]. For example, the state variable vector $\overline{x}^{n_z^i} = [0, 0, 1, 0, 0]$ indicates that the generic z-th node n_z^i

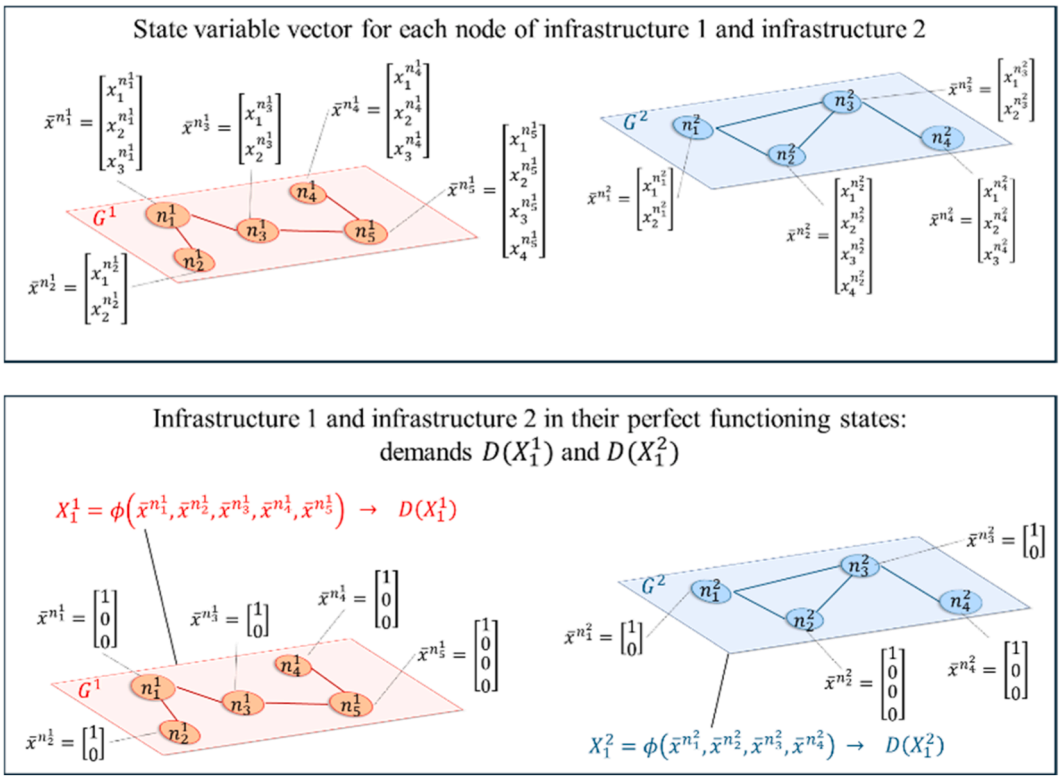

Fig. 5. Characterization of infrastructure 1 and infrastructure 2 of Fig. 1.

of the i-th CI, is in its third state ($x_3^{n_z^i}$).

The state of each node reflects its capability to deliver a specific task. Initially, a node operates under a given load, representing the demand it must meet. As failures propagate, the initial load on a node can increase and, in some cases, exceed its capacity. When this occurs, the node becomes unable to fully meet demand, leading to partial or complete failure. See Appendix A for a procedure to estimate the extent of unmet demand by a generic CI exposed to disruption.

Consequently, the state of the generic i-th CI, G^i, is a function of the states of its nodes N^i and is represented by the CI state variable vector $\overline{X}^i = [X_1^i, X_2^i, \ldots, X_L^i]$, where the generic l-th element, $l = 1, 2, \ldots, L$, is a function of the nodes states variables, $X_l^i = \phi\left(\overline{x}^{n_1^i}, \overline{x}^{n_2^i}, \ldots, \overline{x}^{n_z^i}\right) \in [0, 1]$. Like for the N^i nodes, the states of G^i are mutually exclusive, meaning that the infrastructure can be in only one state at a time. Also, X_1^i corresponds to the perfect functioning state of G^i ($q_i = 0$), and X_L^i represents complete failure ($q_i = 1$).

The inoperability state of a CI corresponds to a physical state of operation with respect to its intended performance. To link inoperability to the CI functioning level, we propose using demand satisfaction as a proxy for the overall operational state [41]. Based on the objective of demand satisfaction, we introduce the function of unmet demand $O(X_l^i)$ as the operational performance metric of the i-th CI, G^i, in state X_l^i, given by:

$$O(X_l^i) = 1 - \frac{D(X_l^i)}{D(X_1^i)} \tag{7}$$

where $D(X_l^i)$ is the demand met by G^i in state X_l^i, and $D(X_1^i)$ is the attended demand of G^i in perfect functioning state X_1^i. When $D(X_l^i) = D(X_1^i)$, G^i is fully functional and $O(X_l^i) = 0$. When $D(X_l^i) = 0$, G^i is unable to meet any demand and $O(X_l^i) = 1$.

Fig. 5 illustrates the characterization phase for the infrastructure 1 and the infrastructure 2 of Fig. 1.

3.3. Mapping of the interdependencies between the multi-state CIs

During the first phase, the focus was on the intra-infrastructure relations among the nodes of each single CI. In this phase, we extend the focus to the system of systems by identifying all the interdependencies between the M CIs. For clarity's sake the bidirectional interdependency ($i \leftrightarrow j$) between the generic G^i and any other generic G^j is referred to as $i \rightarrow j$ and $j \rightarrow i$, when G^i is the independent CI and G^j the dependent CI, or vice versa, respectively. The identification is based on a given taxonomy, such as provided in [42,43]:

- *Physical interdependencies* between G^i and G^j, originating from a direct provision of services or goods from G^i to G^j, or vice versa;
- *Geographical* interdependencies associated to the proximity of geographical location of G^i and G^j, which might expose them to the same hazards;
- *Cyber interdependencies* that arise from the sharing of information between G^i and G^j;
- *Logical interdependencies* that originate from logical relationships or functional linkages between G^i and G^j.

Once an interdependency $i \leftrightarrow j$ is identified, it is included in the topological graph of the system of systems by defining the edges that connect G^i and G^j, $E^{(i,j)} = \left\{e_{ol}^{i,j} = \left(n_o^i, n_l^j\right) \subseteq N^i \times N^j\right\}$ for the dependency $i \rightarrow j$, and for the dependency $j \rightarrow i$, the edges $E^{(j,i)} = \left\{e_{ol}^{j,i} = \left(n_o^j, n_l^i\right) \subseteq N^j \times N^i\right\}$.

The nodes involved in these interdependencies are those in the node sets $N_{i\rightarrow j}^i$, $N_{i\rightarrow j}^j$, $N_{j\rightarrow i}^i$ and $N_{j\rightarrow i}^j$, where $N_{i\rightarrow j}^i \subseteq N^i$ is the set of nodes of G^i responsible for the dependency $i \rightarrow j$, and $N_{i\rightarrow j}^j \subseteq N^j$ is the set of nodes in G^j connected to $N_{i\rightarrow j}^i$, whereas $N_{j\rightarrow i}^j \subseteq N^j$ is the set of nodes of G^j

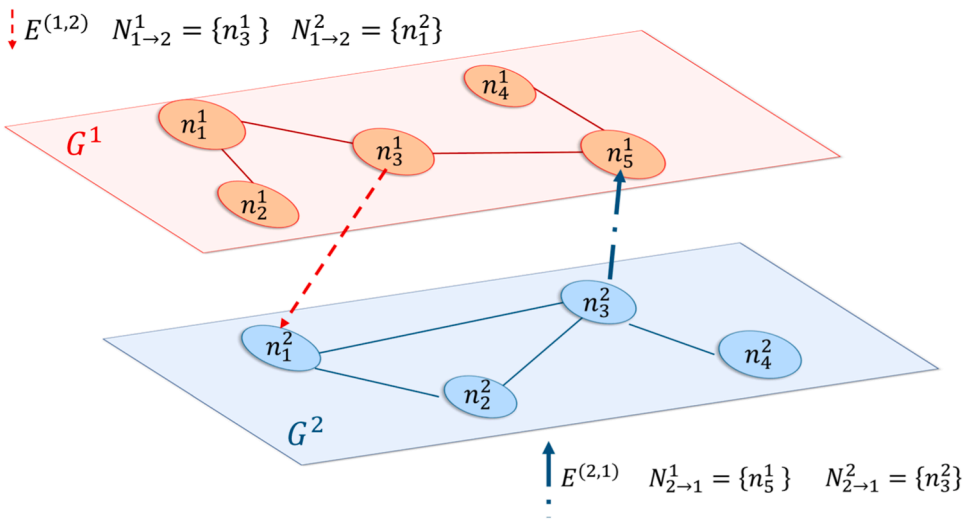

Fig. 6. System of systems: interdependency 1 ↔ 2 (dependencies 1→2 and 2→1).

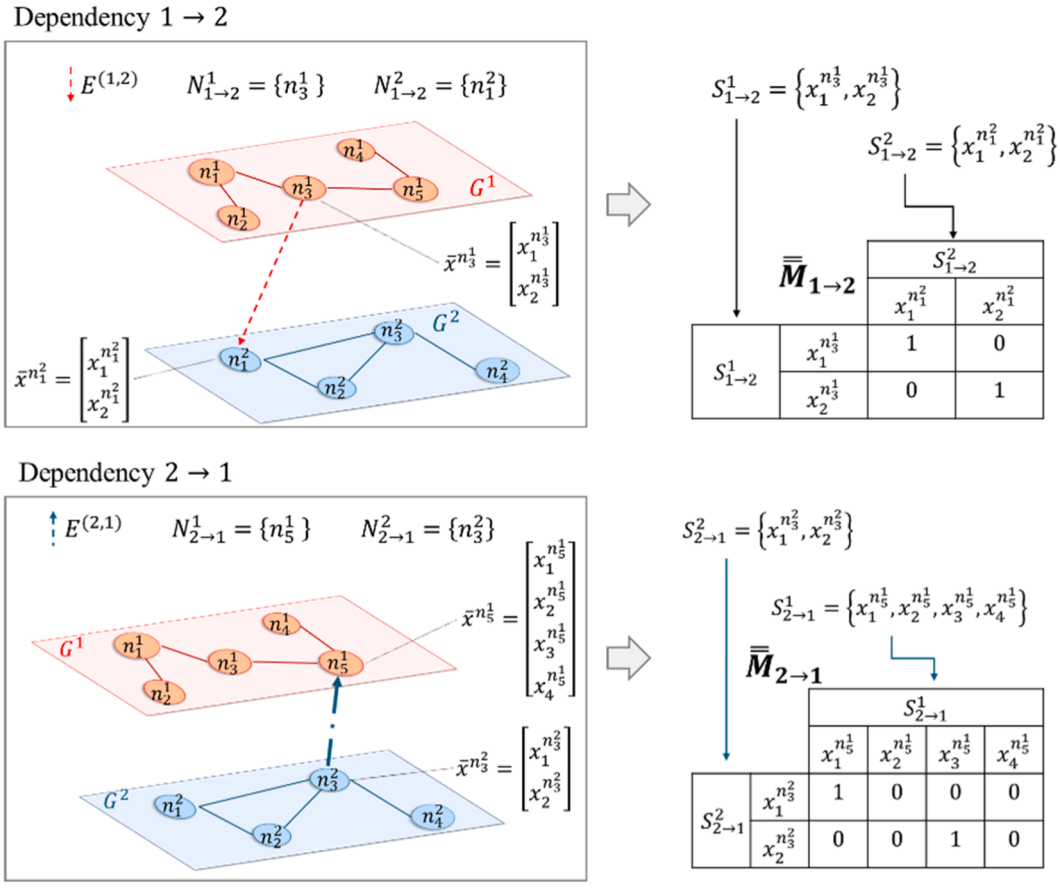

$\bar{\bar{M}}_{1\to2}$		$S^2_{1\to2}$	
		$x_1^{n^2_1}$	$x_2^{n^2_1}$
$S^1_{1\to2}$	$x_1^{n^1_3}$	1	0
	$x_2^{n^1_3}$	0	1

$\bar{\bar{M}}_{2\to1}$		$S^1_{2\to1}$			
		$x_1^{n^1_5}$	$x_2^{n^1_5}$	$x_3^{n^1_5}$	$x_4^{n^1_5}$
$S^2_{2\to1}$	$x_1^{n^2_3}$	1	0	0	0
	$x_2^{n^2_3}$	0	0	1	0

Fig. 7. Matrices $\bar{\bar{M}}_{1\to2}$ and $\bar{\bar{M}}_{2\to1}$.

responsible for the dependency $j\to i$, and $N^i_{j\to i} \subseteq N^i$ is the set of nodes in G^i connected to $N^j_{j\to i}$.

Fig. 6 exemplifies this step for the infrastructures analyzed in Section 2, considering that, according to Fig. 1, there is an interdependency relationship between infrastructure 1 and infrastructure 2. This means that there exists both a dependency 1→2 and a dependency 2→1.

To quantify the effects of the interdependency $i \leftrightarrow j$, we proceed by analyzing to what extent any change in states of the nodes set $N^i_{i\to j}$ causes changes in the states of the nodes set $N^j_{i\to j}$, and vice versa for $N^j_{j\to i}$ and $N^i_{j\to i}$. For each set $N^i_{i\to j}$ and $N^j_{i\to j}$, the sets of node states are identified and denoted as $S^i_{i\to j}$ and $S^j_{i\to j}$, respectively (and similarly $S^j_{j\to i}$ and $S^i_{j\to i}$ for $N^j_{j\to i}$ and $N^i_{j\to i}$). These sets include all possible states of the nodes $N^i_{i\to j}$ and $N^j_{i\to j}$ ($N^j_{j\to i}$, $N^i_{j\to i}$), and are defined as follows:

Inputs for analyzing the dependency $i \rightarrow j$ in scenario s:
Nodes in the i-th CI, N^i
Nodes in the j-th CI, N^j
Nodes in the i-th CI connected to the j-th CI, $N^i_{i\rightarrow j}$
Nodes in the j-th CI connected to the i-th CI, $N^j_{i\rightarrow j}$
Dependency matrix, $\overline{\overline{M}}_{i\rightarrow j}$
Intervals of operational domain of the i-th CI, r^i
Intervals of operational domain of the j-th CI, r^j
Demand met by the i-th CI in perfect state, $D\left(X^i_1\right)$
Demand met by the j-th CI in perfect state, $D\left(X^j_1\right)$

define n_r as a random integer from 1 to $\left|N^i\right|$
select randomly n_r nodes from N^i to form the subset N^i_r
for each node $n^i_z \in N^i_r$:
    update $x^{n^i_z}_1 = 0$ to deactivate the perfect functioning state
    select a random integer k from 2 to $\left|x^{n^i_z}_{K_{n^i_z}}\right|$, choosing a random state other than perfect functioning
    set $x^{n^i_z}_k = 1$ to activate the randomly chosen state
end
set $X^i_{s^o}$ as the initial state condition s^o in the i-th CI
run operational disruption in the i-th CI
define s^f as the final state of nodes in N^i
define $X^i_{s^f}$ as the final state of the i-th CI
set $D\left(X^i_{s^f}\right)$ as the met demand of the i-th CI in state $X^i_{s^f}$
set $O\left(X^i_{s^f}\right)$ as the operational performance of the i-th CI for scenario s
determine the interval r^i_e from r^i such that $a_e \le O\left(X^i_{s^f}\right) \le b_e$
store r^i_e
for each node $n^j_z \in N^j_{i\rightarrow j}$:
    update $\bar{x}^{n^j_z}$ according to $\overline{\overline{M}}_{i\rightarrow j}$
end
set $X^j_{c^o}$ as the initial state conditions c^o in the j-th CI
run operational disruption in the j-th CI
define c^f as the final state of nodes in N^j
define $X^j_{c^f}$ as the final state of the j-th CI
set $D\left(X^j_{c^f}\right)$ as the met demand of the j-th CI in state $X^j_{c^f}$
set $O\left(X^j_{c^f}\right)$ as the operational performance of the j-th CI for scenario s
determine the interval r^j_l from r^j such that $c_l \le O\left(X^j_{c^f}\right) \le d_l$
store r^j_l

Output: r^i_k and r^j_l, operational performance ranges for the i-th CI and the j-th CI under scenario s, respectively

Fig. 8. Pseudocode to analyze the dependency $i \rightarrow j$ under scenario s.

$$
\begin{aligned}
S^i_{i\rightarrow j} &= \left\{ x^{n^i_z}_k \middle| n^i_z \in N^i_{i\rightarrow j}, \quad x^{n^i_z}_k \in \bar{x}^{n^i_z} \text{ for } k = 1, \ldots, K_{n^i_z} \right\} \\
S^j_{i\rightarrow j} &= \left\{ x^{n^j_z}_k \middle| n^j_z \in N^j_{i\rightarrow j}, \quad x^{n^j_z}_k \in \bar{x}^{n^j_z} \text{ for } k = 1, \ldots, K_{n^j_z} \right\} \\
S^i_{j\rightarrow i} &= \left\{ x^{n^i_z}_k \middle| n^i_z \in N^i_{j\rightarrow i}, \quad x^{n^i_z}_k \in \bar{x}^{n^i_z} \text{ for } k = 1, \ldots, K_{n^i_z} \right\} \\
S^j_{j\rightarrow i} &= \left\{ x^{n^j_z}_k \middle| n^j_z \in N^j_{j\rightarrow i}, \quad x^{n^j_z}_k \in \bar{x}^{n^j_z} \text{ for } k = 1, \ldots, K_{n^j_z} \right\}
\end{aligned}
\tag{8}
$$

$S^i_{i\rightarrow j}$ and $S^j_{i\rightarrow j}$ are used to create the dependency matrix $\overline{barM}_{i\rightarrow j}$, where the rows correspond to elements in $S^i_{i\rightarrow j}$ and the columns correspond to elements in $S^j_{i\rightarrow j}$. If a state in the row can lead to a state in the column, the value at that row and column is 1; otherwise, it is 0. Similarly, $S^j_{j\rightarrow i}$ and $S^i_{j\rightarrow i}$ are used to create $\overline{barM}_{j\rightarrow i}$. For the example of the interdependency relationships shown in Fig. 6, two matrices $\overline{barM}_{1\rightarrow 2}$ and $\overline{barM}_{2\rightarrow 1}$ are created as illustrated in Fig. 7.

The matrix $\overline{barM}_{1\rightarrow 2}$ maps the effect on the state of node n^2_1 due to a change in the state of node n^1_3, when node n^1_3 becomes inoperable ($x^{n^1_3}_2 = 1$), the inoperability propagates to infrastructure 2, causing n^2_1 to also become inoperable ($x^{n^2_1}_2 = 1$). Similarly, for the dependency 2→1, the matrix $\overline{barM}_{2\rightarrow 1}$ shows that when node n^2_3 reaches its inoperability state ($x^{n^2_3}_2 = 1$), node n^1_5 achieves a partially inoperable state ($x^{n^1_5}_3 = 1$) thanks to its robustness that prevents it reaching full inoperability and mitigating the propagation of inoperability to infrastructure 1.

While this study focuses on physical interdependencies, the proposed methodology can be extended to other types of interdependencies with appropriate modifications to the respective dependency matrices ($\overline{barM}_{i\rightarrow j}$, $\overline{barM}_{j\rightarrow i}$): for geographical interdependencies, the matrices must capture shared risk exposure to hazard events, ensuring that nodes in the same location undergo the same state transitions; for cyber interdependencies, the dependency matrices can be structured so that inoperability propagates through disrupted communication links, where attacks to one CI node affects its connected nodes in another CI; for logical interdependencies, rule-based dependencies can be introduced, modifying the dependency matrices to reflect constraints in which the failure of a node in one CI directly limits the functionality of another node in the dependent CI according to predefined rules. By adjusting the

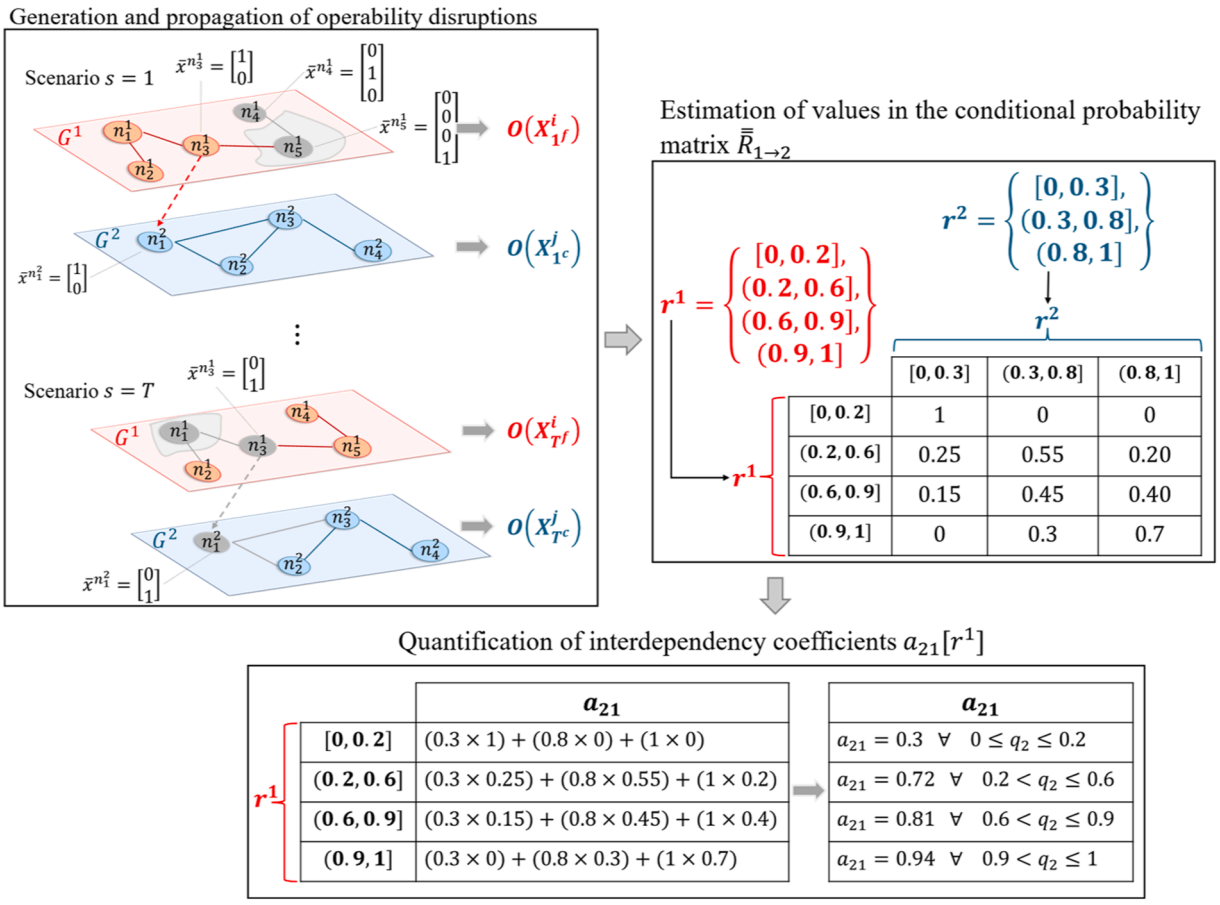

r^1 \ r^2	[0, 0.3]	(0.3, 0.8]	(0.8, 1]
[0, 0.2]	1	0	0
(0.2, 0.6]	0.25	0.55	0.20
(0.6, 0.9]	0.15	0.45	0.40
(0.9, 1]	0	0.3	0.7

r^1	a_{21}	a_{21}
[0, 0.2]	(0.3 × 1) + (0.8 × 0) + (1 × 0)	$a_{21} = 0.3 \quad \forall \quad 0 \le q_2 \le 0.2$
(0.2, 0.6]	(0.3 × 0.25) + (0.8 × 0.55) + (1 × 0.2)	$a_{21} = 0.72 \quad \forall \quad 0.2 < q_2 \le 0.6$
(0.6, 0.9]	(0.3 × 0.15) + (0.8 × 0.45) + (1 × 0.4)	$a_{21} = 0.81 \quad \forall \quad 0.6 < q_2 \le 0.9$
(0.9, 1]	(0.3 × 0) + (0.8 × 0.3) + (1 × 0.7)	$a_{21} = 0.94 \quad \forall \quad 0.9 < q_2 \le 1$

Fig. 9. Estimation of interdependency coefficient a_{21}.

formulation of $\overline{barM}_{i\to j}$ and $\overline{barM}_{j\to i}$ accordingly, the methodology remains adaptable to different interdependency types while preserving its core structure.

3.4. Estimating interdependency coefficients

To estimate the interdependency coefficients a_{ji} due to $i\to j$, and a_{ij} due to $j\to i$, we simulate T operability disruption scenarios in the i-th CI and analyze their effects on the j-th CI, and vice versa.

The failure propagation in each disruption scenario follows the procedure detailed in Appendix A. In this sense, inoperability of nodes is inherently linked to their physical conditions, such as initial load and capacity, reflecting real-world conditions where exceeding node capacity can amplify cascading effects in interdependent CIs.

As we shall see in what follows, more severe disruptions occurring in the i-th CI generate more significant impacts on the j-th CI operability, and similarly for those occurring in the j-th CI impacting the i-th CI.

The outcomes of the simulations allow for the evaluation of the operational performance metric in Eq. (7), resulting in an inoperability metric that is not binary but discretized into multiple intervals within $[0, 1]$ for both the i-th CI and the j-th CI; this enables a more granular analysis of the relationships between the different operability states of the CIs.

In practice, let the inoperability domain $[0, 1]$ for the i-th CI be divided into intervals $r_e^i = \{[a_e, b_e]\}$ for $e = 1,\ldots,r^i$, where $0 = a_1 < b_1 = a_2 < b_2 = \ldots = a_{r^i} < b_{r^i} = 1$. Similarly, the inoperability domain $[0, 1]$ for the j-th CI is divided into intervals $r_l^j = \{[c_l, d_l]\}$ for $l = 1,\ldots,r^j$, where $0 = c_1 < d_1 = c_2 < d_2 = \ldots = c_{r^j} < d_{r^j} = 1$.

The values of the intervals r_e^i and r_l^j define the rows and columns of the conditional probability matrix $\bar{\bar{R}}_{i\to j}$, and the columns and rows of the conditional probability matrix $\bar{\bar{R}}_{j\to i}$, respectively. Each entry of these matrices is the probability that the inoperability of the dependent infrastructure (j/i) is in a specific inoperability interval (r_l^j/r_e^i), given that the inoperability of the independent infrastructure (i/j) is in a specific inoperability interval (r_e^i/r_l^j).

Monte Carlo simulation is used to generate the set of T scenarios (the pseudocode is given in Fig. 8 for $i\to j$). For each scenario s $(s = 1,\ldots,T)$, the initial states s^o of G^i, $X_{s^o}^i$, are set by random generation of operational disruptions, i.e., by uniform random sampling n_r nodes from N^i to form the subset N_r^i, and by uniform random sampling their inoperability states $x_k^{n_z^i} = 1,\ k \ne 1\ \forall n_z^i \in N_r^i$.

The disruption is, then, propagated through the i-th CI (for example as proposed by [44] and [45]), and the operational performance of G^i is estimated based on the final state of the nodes N^i of G^i, which reaches the final s^f state, $X_{s^f}^i$. The operational performance for the i-th CI $(O(X_{s^f}^i))$ is, then, calculated as in Eq. (7), classified in the appropriate range r_e^i and recorded. The final state $X_{s^f}^i$ of the i-th CI cascades on the j-th CI, as defined by the matrix $\overline{barM}_{i\to j}$, whose initial nodes states $X_{c^o}^j$ of the set $N_{i\to j}^j$, denoted as c^0, reach the final state $X_{c^f}^j$, whose performance $O\left(X_{c^f}^j\right)$ is classified in the appropriate column range r_l^j. From the T simulations, the frequencies of occurrence of each inoperability interval of the i-th CI (row in $\bar{\bar{R}}_{i\to j}$), for each corresponding inoperability interval of the j-th CI (column in $\bar{\bar{R}}_{i\to j}$) are calculated to estimate the corresponding entry of

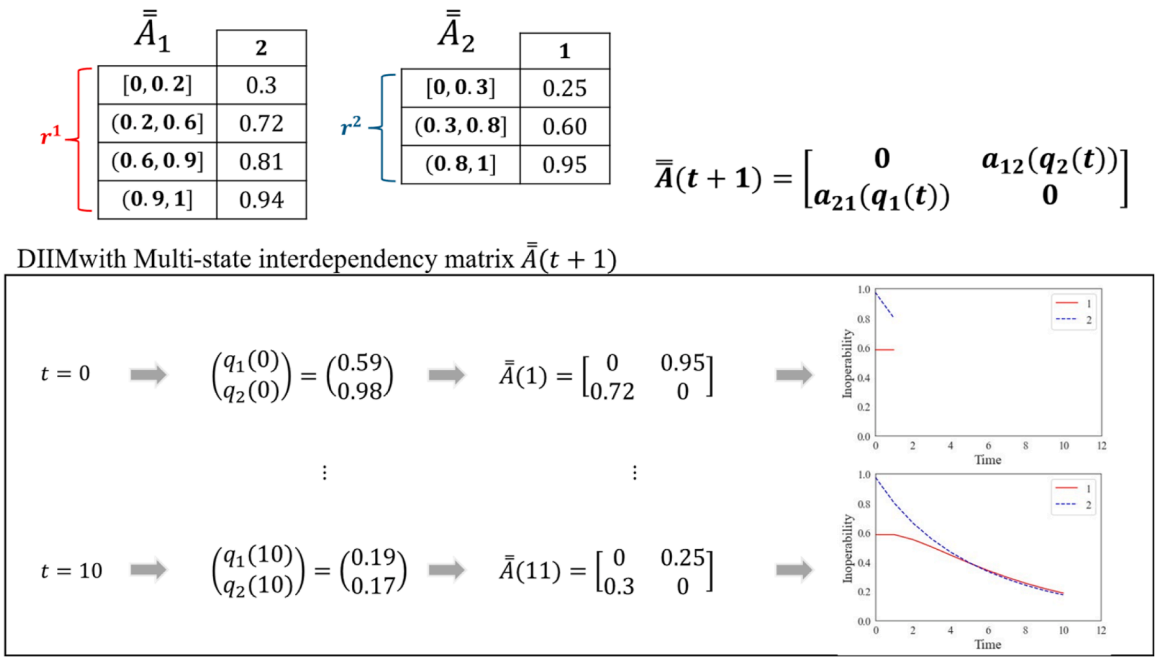

Fig. 10. DIIM with multi-state interdependency matrix for interdependency $1 \leftrightarrow 2$.

$\bar{\bar{R}}_{i\to j}$. Similarly, Monte Carlo sampling are used to estimate the frequency of the elements of $\bar{\bar{R}}_{j\to i}$ for the dependency $j\to i$, using the corresponding intervals and initial conditions set in the nodes N^j of the generic j-th CI, G^j, and propagating the disruption effects back to the i-th CI as defined by the matrix $\overline{barM}_{j\to i}$.

The frequency-estimated elements of $\bar{\bar{R}}_{i\to j}$ for the dependency $i\to j$ represent the probabilities of the j-th CI being in each of its inoperability intervals (columns), given that the i-th CI is in the corresponding row interval, expressed as:

$$P\left(O(X_u^j) \in r_l^j \middle| O\left(X_p^i\right) \in r_e^i\right) \tag{9}$$

where $P\left(O(X_u^j) \in r_l^j \middle| O\left(X_p^i\right) \in r_e^i\right)$ is the conditional probability that the operational performance of the j-th CI in a disrupted state denoted as X_u^j falls within the range r_l^j, given that the operational performance of the i-th CI, represented by $O\left(X_p^i\right)$ for the disrupted state X_p^i, is within the range r_e^i.

Likewise, for the dependency $j\to i$, the frequency-estimated elements of $\bar{\bar{R}}_{j\to i}$ represent the probabilities of the i-th CI being in each of its inoperability ranges (columns), given that the j-th CI is in the inoperability ranges corresponding to the row interval:

$$P\left(O(X_u^i) \in r_e^i \middle| O\left(X_p^j\right) \in r_l^j\right) \tag{10}$$

where $P\left(O(X_u^i) \in r_e^i \middle| O\left(X_p^j\right) \in r_l^j\right)$ is the conditional probability that the operational performance of the i-th CI in a disrupted state denoted as X_u^i falls within the range r_e^i, given that the operational performance of the j-th CI, represented by $O\left(X_p^j\right)$ for the disrupted state X_p^j, is within the range r_l^j.

Finally, the interdependency coefficients $a_{ji}(r_e^i)\ \forall r_e^i \in r^i$ and $a_{ij}\left(r_l^j\right)\ \forall r_l^j \in r^j$ are calculated as:

$$\begin{aligned} a_{ji}(r_e^i) &= \sum_{l=1}^{r^j} P\left(O(X_u^j) \in r_l^j \middle| O\left(X_p^i\right) \in r_e^i\right) \cdot d_l \\ a_{ij}\left(r_l^j\right) &= \sum_{e=1}^{r^i} P\left(O(X_u^i) \in r_e^i \middle| O\left(X_p^j\right) \in r_l^j\right) \cdot b_e \end{aligned} \tag{11}$$

where d_l corresponds to the upper limit of the range r_l^j, defining the maximum potential impact on the j-th CI's operational performance, and b_e corresponds to the upper limit of the range r_e^i, defining the maximum potential impact on the i-th CI's operational performance.

Fig. 9 exemplifies the estimation of interdependency coefficient a_{21} for the dependency $(2\to1)$ between infrastructure 1 and infrastructure 2 shown in Fig. 4. For infrastructure 1, four intervals are defined: $r^1 = \{[0, 0.2], (0.2, 0.6], (0.6, 0.9], (0.9, 1]\}$, and for infrastructure 2, three intervals are created: $r^2 = \{[0, 0.3], (0.3, 0.8], (0.8, 1]\}$. The Monte Carlo sampling yield $\bar{\bar{R}}_{1\to2}$, enabling the estimation of interdependency coefficient a_{21} for each interval of infrastructure 1. For example, in the interval $(0.2, 0.6]$, the probabilities of infrastructure 2 being in the inoperability ranges $[0, 0.3]$, $(0.3, 0.8]$, and $(0.8, 1]$ are 0.35, 0.55, and 0.10, respectively. Thus, the interdependency coefficient $a_{21}(0.2, 0.6]$, representing the inoperability contribution from infrastructure 1 to infrastructure 2 when infrastructure 1 is inoperable between 0.2 and 0.6, is calculated as:

$$a_{21}(0.2, 0.6] = 0.35 \times 0.3 + 0.55 \times 0.8 + 0.1 \times 1 = 0.65 \tag{12}$$

For the generic i-th CI, the matrix $\bar{\bar{A}}_i$ is finally obtained, where each row corresponds to the inoperability intervals r^i and the columns to all the CIs that depend on the i-th CI. Similarly, for the j-th CI, $\bar{\bar{A}}_j$ contains the interdependency coefficients of the other CIs that depend on the j-th CI.

The DIIM of Eq. (4) can be ultimately applied, fed by the multi-state interdependency matrix $\bar{\bar{A}}(t+1)$, which updates based on the actual inoperability values of the CIs at time t. Fig. 10 exemplifies the DIIM application for the interdependency $i \leftrightarrow j$.

4. Case study

We present a case study concerning a system of systems made by an

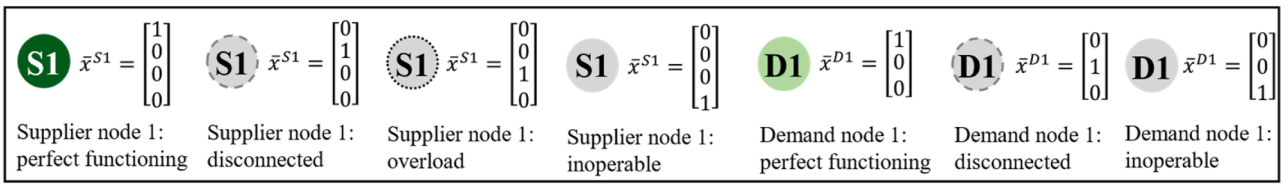

Fig. 11. States of supplier and demand nodes.

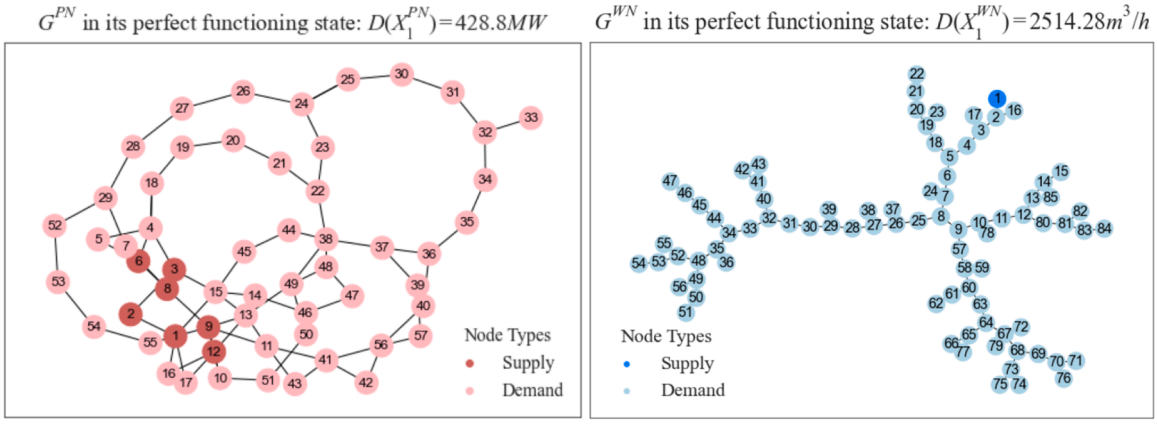

Fig. 12. Characterization of $\boldsymbol{G^{PN}}$ and $\boldsymbol{G^{WN}}$.

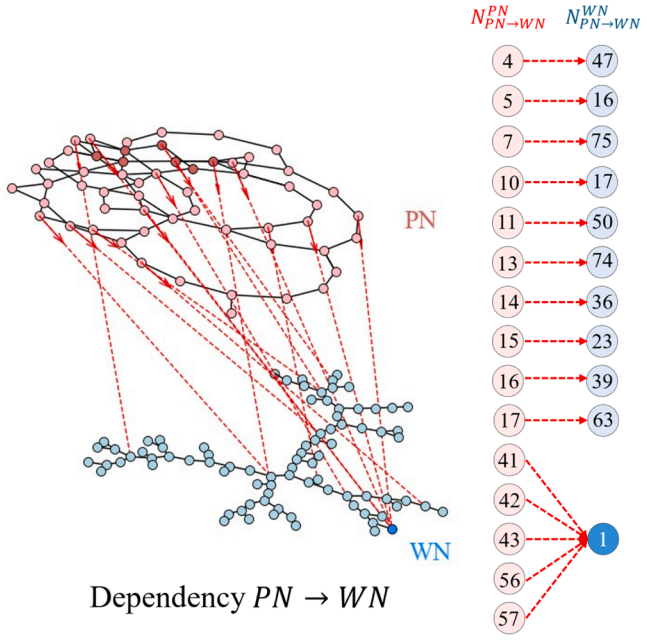

Fig. 13. System of systems: dependency $\boldsymbol{PN \to WN}$.

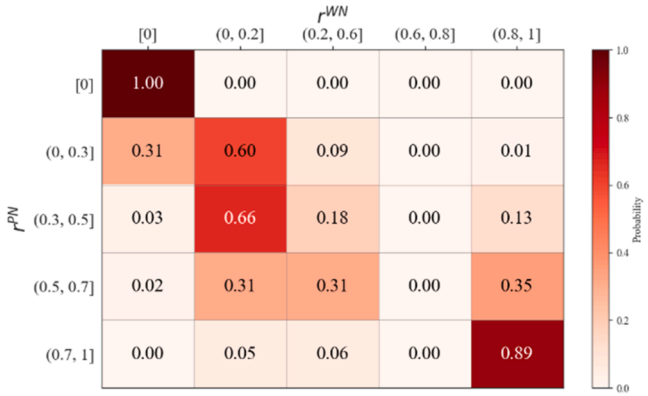

Fig. 14. Conditional probability matrix $\overline{\overline{\boldsymbol{R}}}_{\boldsymbol{PN\to WN}}$.

interdependent water CI and power CI: the power network (PN) is based on the IEEE57-bus test system and the water supply network (WN) topology is taken from the IEEE85-bus system of [46].

We distinguish the nodes of these CIs as supplier and demand nodes, based on their role in the flow of commodities [47,48]. In the PN, supplier nodes represent power plants or substations that generate or distribute electricity, whereas demand nodes correspond to loads such as homes, businesses, water treatment plants and pumping stations. In the WN, supplier nodes are water treatment facilities that provide clean water, and demand nodes represent residential, commercial and industrial users, as well as pumping stations that distribute it further [49].

Supplier nodes can be in one of four states: perfect functioning, disconnected (due to loss of edges connecting to demand nodes), overloaded (required to supply more than capacity) or inoperable. Demand nodes can be in one of three states: perfect functioning, disconnected (due to loss of edges connecting to supplier nodes) or inoperable (illustrated in Fig. 11). Note that it is important to distinguish between the states 'inoperable' and 'disconnected', because the recovery action related to the former requires maintenance or repair, whereas the recovery of a disconnection amounts to connecting or reconnecting neighbor nodes of the disconnected node.

The PN topology, denoted as G^{PN}, includes seven supply nodes providing electricity to fifty demand nodes. In its perfect functioning state, X_1^{PN}, it meets a demand of $D(X_1^{PN}) = 428.8$ MW. The WN, denoted as G^{WN}, in its perfect functioning state X_1^{WN} delivers $D(X_1^{WN}) = 2514.28$ m^3/h of water from one supply node to eighty-four demand nodes. Fig. 12 shows the topological structure of G^{PN} and G^{WN}. Appendix B details the demand for each demand node, as well as the initial load and capacity of the supplier nodes in each CI.

As said, PN and WN are interdependent, i.e., $PN \leftrightarrow WN$: in the

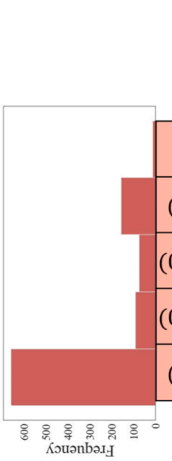

r^{PN} \ r^{WN}	[0]	(0, 0.2]	(0.2, 0.6]	(0.6, 0.8]	(0.8, 1]	$a_{WNPN}[r_k^{PN}]$
[0]	1 × 0	0 × 0.2	0 × 0.6	0 × 0.8	0 × 1	0
(0, 0.3]	0.31 × 0	0.60 × 0.2	0.09 × 0.6	0 × 0.8	0.01 × 1	0.18
(0.3, 0.5]	0.03 × 0	0.66 × 0.2	0.18 × 0.6	0 × 0.8	0.13 × 1	0.37
(0.5, 0.7]	0.02 × 0	0.31 × 0.2	0.31 × 0.6	0 × 0.8	0.35 × 1	0.60
(0.7, 1]	0 × 0	0.05 × 0.2	0.06 × 0.6	0 × 0.8	0.89 × 1	0.94

Fig. 15. Interdependency coefficient estimation $a_{WNPN}(r_k^{PN})\ \forall k \in r^{PN}$.

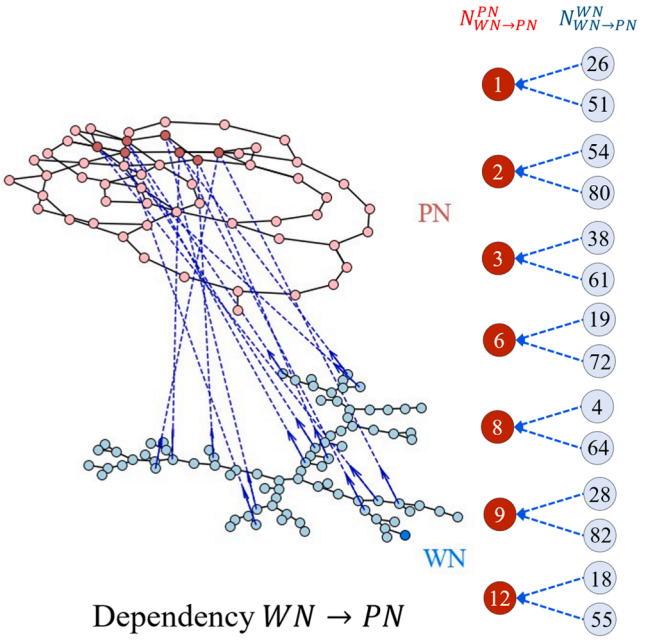

Fig. 16. System of systems: dependency ***WN→PN***.

following, such dependencies are described in detail.

4.1. Dependency of water network on power network: PN→WN

The dependency *PN→WN* means that water treatment and distribution processes require electricity to function. To model *PN→WN*, 15 nodes in G^{PN} supply 11 demand nodes in G^{WN}. The nodes involved are as follows:

$$N^{PN}_{PN\to WN} = \left\{ \begin{matrix} n^{PN}_4, n^{PN}_5, n^{PN}_7, n^{PN}_{10}, n^{PN}_{11}, n^{PN}_{13}, n^{PN}_{14}, n^{PN}_{15}, n^{PN}_{16}, n^{PN}_{17}, \\ n^{PN}_{41}, n^{PN}_{42}, n^{PN}_{43}, n^{PN}_{56}, n^{PN}_{57} \end{matrix} \right\}$$
$$N^{WN}_{PN\to WN} = \left\{ \begin{matrix} n^{WN}_1, n^{WN}_{16}, n^{WN}_{17}, n^{WN}_{23}, n^{WN}_{36}, n^{WN}_{39}, n^{WN}_{47}, n^{WN}_{50}, n^{WN}_{63}, \\ n^{WN}_{74}, n^{WN}_{75} \end{matrix} \right\} \quad (13)$$

The number of nodes differs between the sets $N^{PN}_{PN\to WN}$ and $N^{WN}_{PN\to WN}$ because five power supply nodes are required to ensure continuous electricity supply to a single supplier node in the WN, as illustrated in Fig. 13.

To map the effects on G^{WN} of the dependency *PN→WN*, the state relations between nodes in $N^{PN}_{PN\to WN}$ with nodes in $N^{WN}_{PN\to WN}$ are analyzed. The direct effects of propagation occur through the specific connections between nodes, i.e., each node in $N^{PN}_{PN\to WN}$ directly influences only the nodes in $N^{WN}_{PN\to WN}$ to which it is directly connected.

All nodes in $N^{PN}_{PN\to WN}$ are multi-state demand nodes: perfect functioning, disconnected or inoperable. Cascading effects in G^{WN} due to inoperability disruptions in G^{PN} occur when nodes in $N^{PN}_{PN\to WN}$ are in a state other than perfect functioning. Consequently, the unavailability of these demand nodes causes the connected nodes in G^{WN} to transition from perfect functioning to any inoperability state.

The inoperability states of nodes in $N^{WN}_{PN\to WN}$ follow specific rules. Demand nodes become inoperable when their corresponding nodes in $N^{PN}_{PN\to WN}$ are in any inoperability state (disconnected or inoperable). The supplier node in $N^{WN}_{PN\to WN}$, supported by five dedicated nodes in $N^{PN}_{PN\to WN}$, becomes inoperable only when all five nodes are in any inoperability state (disconnected or inoperable).

To estimate the interdependency coefficient a_{WNPN}, the inoperability domain of each CI is divided into five intervals with increasing inoperability values, as follows.

$$r^{PN} = \{[0],\ (0,\ 0.3],\ (0.3,\ 0.5],\ (0.5, 0.7], (0.7, 1]\}$$
$$r^{WN} = \{[0],\ (0,\ 0.2],\ (0.2,\ 0.6],\ (0.6, 0.8], (0.8, 1]\} \quad (14)$$

Then, the conditional probability matrix $R_{PN\to WN}$ of Fig. 14 is calculated, with rows corresponding to r^{PN} and columns to r^{WN}. To estimate these values a Monte Carlo sampling with $T = 1000$ runs is performed according to the pseudocode of Fig. 8.

The interdependency coefficients for each inoperability range of PN ($a_{WNPN}[r_k^{PN}],\ \forall r_k^{PN} \in r^{PN}$) are calculated and reported in Fig. 15 (last column) by using Eq. (11) and the frequencies plotted in the histogram (left of Fig. 15).

4.2. Dependency of power network on water network: WN→PN

Cooling and other essential processes in power plants and substations rely on water supply. To represent the dependency of PN on WN (*WN→PN*), in this case study, we select 14 nodes in G^{WN} as water suppliers to the 7 power supplier nodes in G^{PN}. The nodes involved are as follows:

$$N^{PN}_{WN\to PN} = \{n^{PN}_1, n^{PN}_2, n^{PN}_3, n^{PN}_6, n^{PN}_8, n^{PN}_9, n^{PN}_{12}\}$$
$$N^{WN}_{WN\to PN} = \left\{ \begin{matrix} n^{WN}_4, n^{WN}_{18}, n^{WN}_{19}, n^{WN}_{26}, n^{WN}_{28}, n^{WN}_{38}, n^{WN}_{51}, n^{WN}_{54}, n^{WN}_{55}, \\ n^{WN}_{61}, n^{WN}_{64}, n^{WN}_{72}, n^{WN}_{80}, n^{WN}_{82} \end{matrix} \right\} \quad (15)$$

The nodes in the set $N^{WN}_{WN\to PN}$ are double of those in $N^{PN}_{WN\to PN}$ because

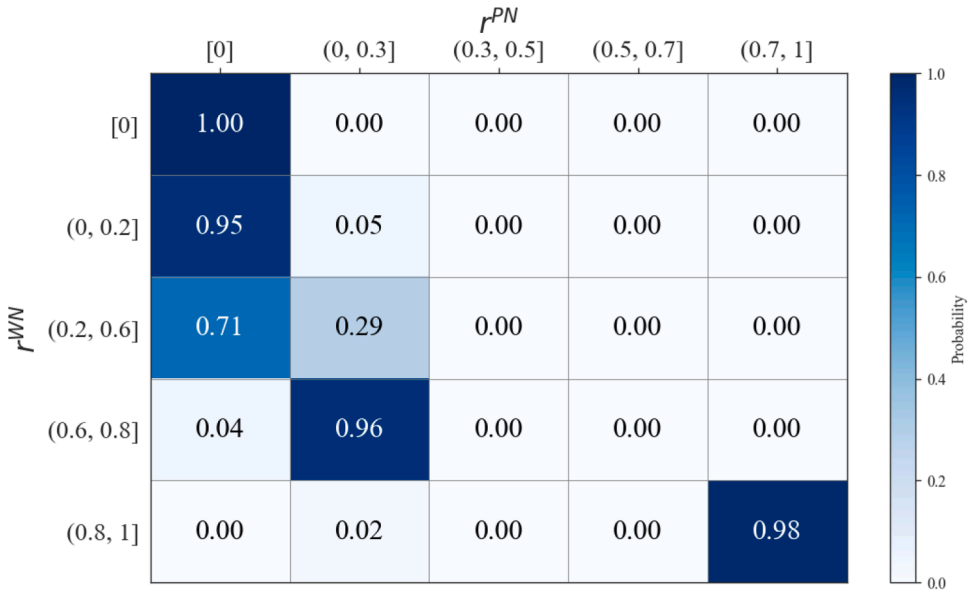

Fig. 17. Conditional probability matrix $\overline{\overline{R}}_{WN \to PN}$.

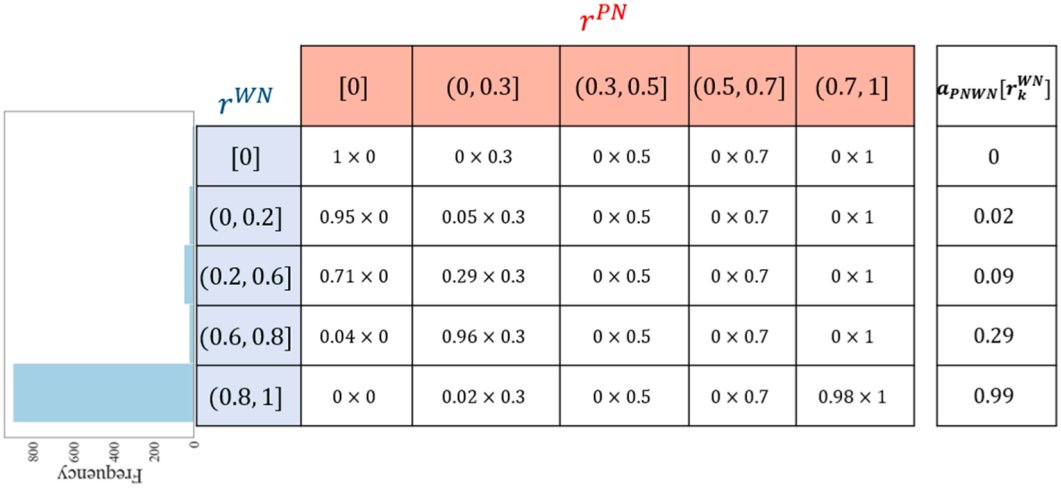

Fig. 18. Interdependency coefficient estimation $a_{PNWN}(r_k^{WN})\ \forall k \in r^{WN}$.

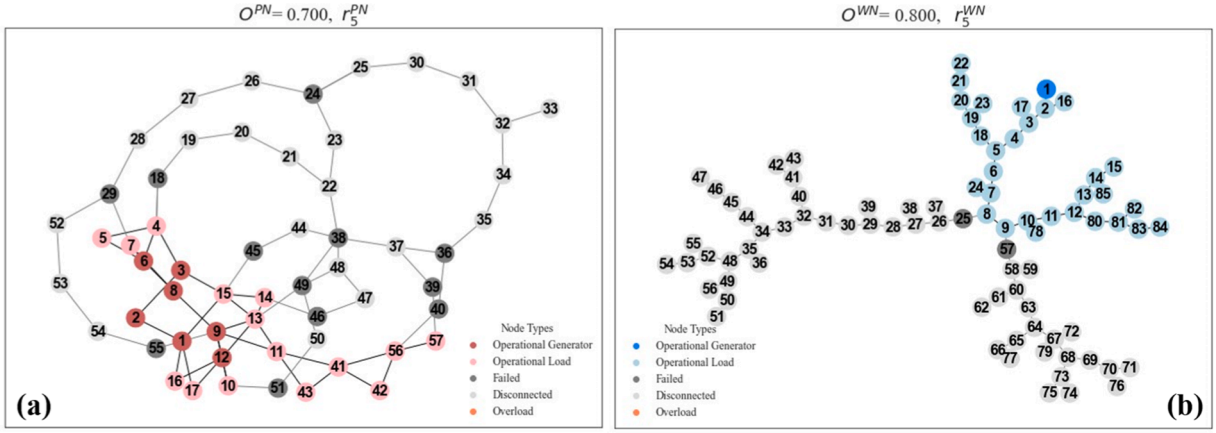

Fig. 19. Examples of disruption operational scenarios resulting in r_5^{PN} (a), and r_5^{WN} (b).

Table 1
Inoperability estimation for two perturbation scenarios.

	IIM based on $\overline{\overline{A}}$ $q_{WN} = (0.93 \times q_{PN} + c_{WN})$	IIM based on $\overline{\overline{A}}(t+1)$ $q_{WN} = (a_{WNPN}(q_{PN}(0)) \times q_{PN} + c_{WN})$
Medium impact $q_{PN} = 0.5$	$q_{WN} = (0.47)$	$q_{WN} = (0.19)$
High impact $q_{PN} = 0.8$	$q_{WN} = (0.74)$	$q_{WN} = (0.74)$

the water supply nodes to PN are redundant, i.e., each node in PN is supplied by two nodes from WN. This is illustrated in Fig. 16, where it is seen that the redundant water supply nodes are not geographically close to each other, so as to reduce the risk of losing water supply to PN nodes due to a local disruption in the WN.

Like the dependency *PN→WN*, the propagation of the direct effects from G^{WN} to G^{PN} occurs through the direct links between nodes in $N^{WN}_{WN\to PN}$ and nodes in $N^{PN}_{PN\to WN}$, i.e., cascading failures are observed in G^{PN} from G^{WN} when nodes in $N^{WN}_{WN\to PN}$ are not in perfect functioning state. This leads the corresponding nodes in $N^{PN}_{PN\to WN}$ to transition from perfect functioning to inoperable state. Particularly, in this case study, nodes in $N^{PN}_{WN\to PN}$ become inoperable only when they lose both redundant water supply nodes that should provide water to them.

Following the methodology presented, Monte Carlo simulation is used to estimate the interdependency coefficients a_{PNWN} for each inoperability interval of WN ($\forall r^{WN}_i \in r^{WN}$), as defined in Eqs. (14). Fig. 17 shows the conditional probability matrix $R_{WN\to PN}$, obtained following the pseudocode outlined in Fig. 8, with $T = 1000$ iterations.

Finally, the interdependency coefficients for each inoperability range of WN ($a_{PNWN}[r^{WN}_k]$, $\forall r^{WN}_k \in r^{WN}$) are determined and presented in the last column of Fig. 18. These values are calculated using Eq. (11) and the frequencies shown in the histogram on the left of Fig. 18.

The computation of interdependency coefficients was performed on an Intel Core i5-11400H CPU with 16 GB RAM. The Monte Carlo simulation with 1000 iterations required 92.82 seconds for $a_{WNPN}(r^{PN}_k)$ and 89.61 seconds for $a_{PNWN}(r^{WN}_k)$.

5. Results and discussion

This section presents the results of the proposed methodology to assess the inoperability dynamics of the interdependent CIs described in the case study. The analysis is structured as follows: Section 5.1 compares the outcomes of the DIIM and the Multi-state DIIM. Section 5.2 focuses on identifying critical nodes within the system of systems, specifically those driving cascading effects between CIs. Section 5.3 evaluates mitigation strategies, highlighting the impact of resilience investments that CI owners can adopt to reduce inoperability.

5.1. Comparison between DIIM and Multi-state DIIM

The inoperability of the CIs described in Section 4 is evaluated using the multi-state interdependent matrix (Eq. (16)):

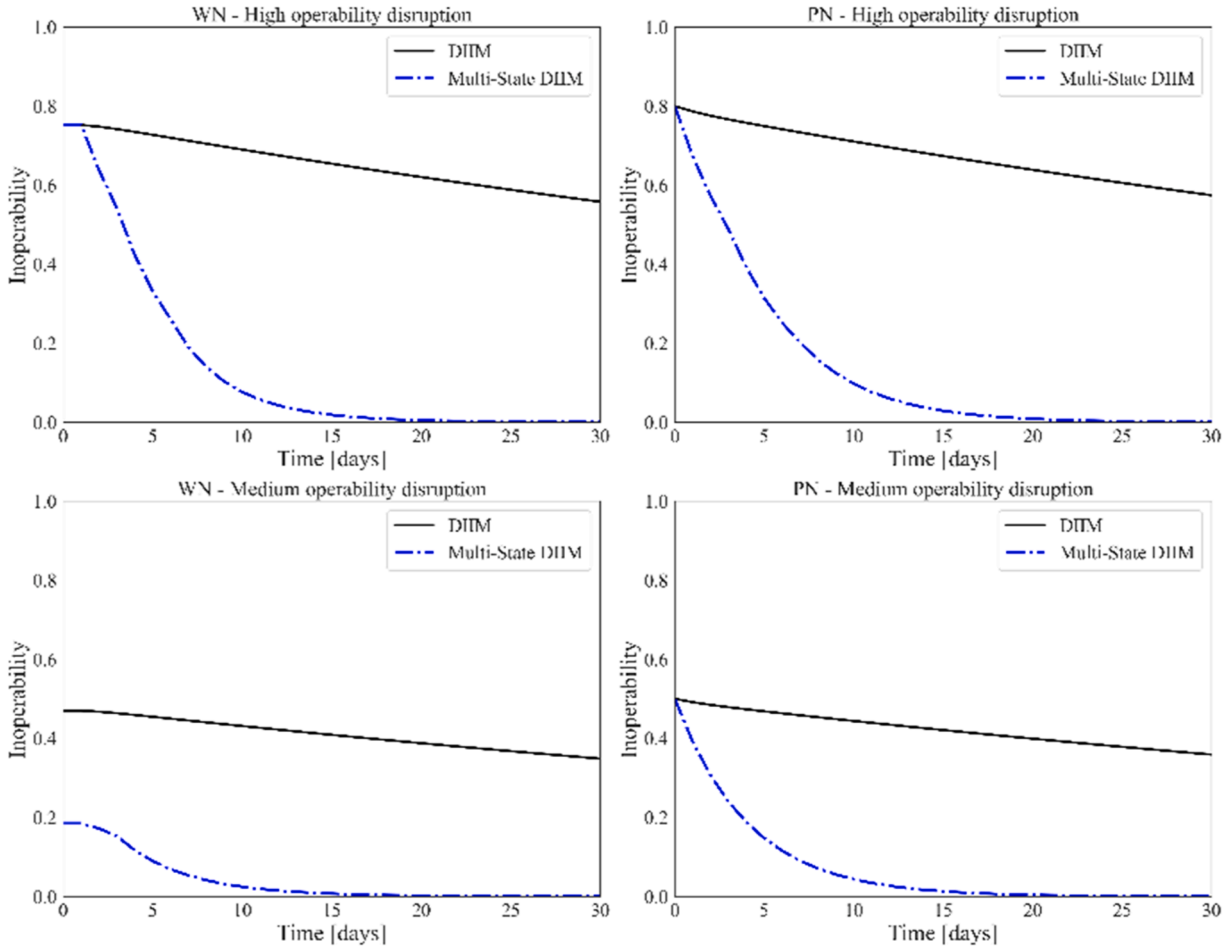

Fig. 20. DIIM vs Multi-state DIIM for two perturbation scenarios.

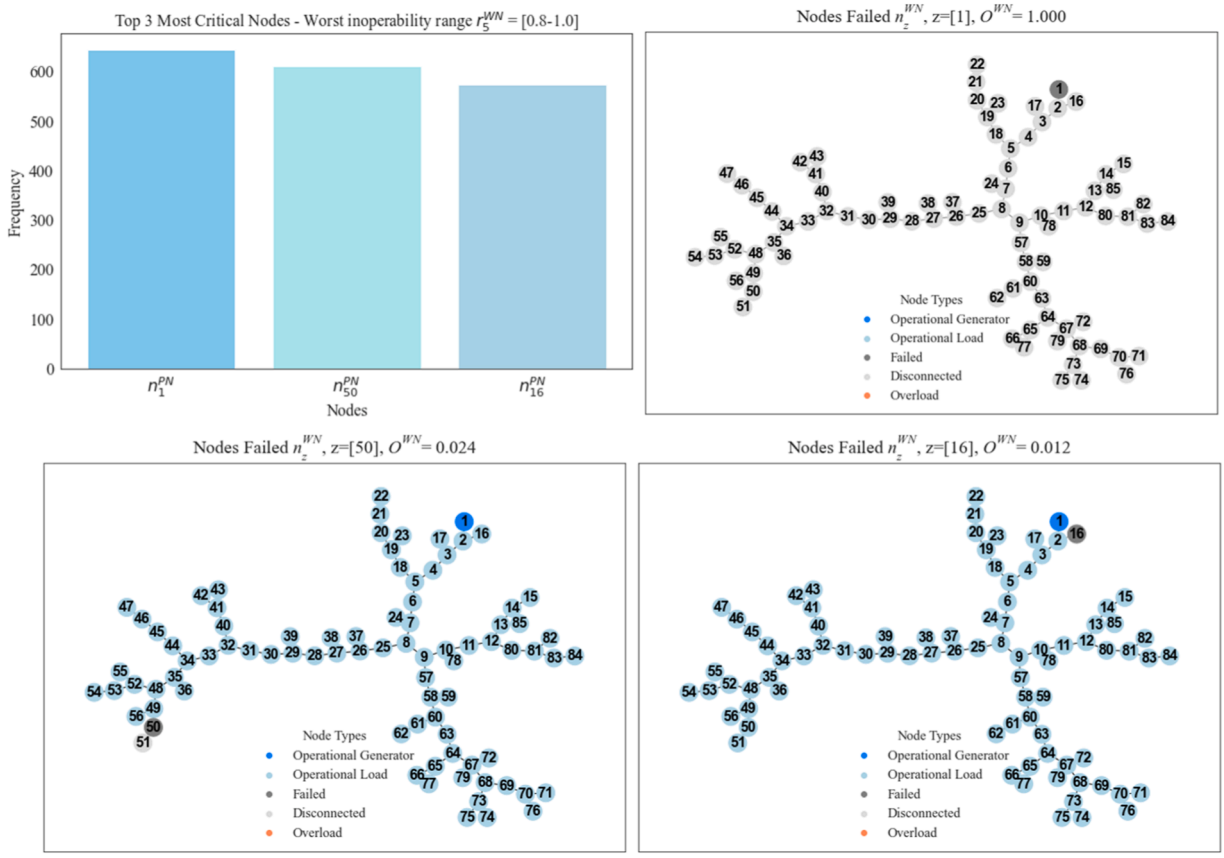

Fig. 21. Dependency ***PN→WN***: analysis of critical nodes in $\boldsymbol{G^{WN}}$.

$$\overline{\overline{A}}(t+1) = \begin{pmatrix} 0 & a_{WNPN}(q_{PN}(t)) \\ a_{PNWN}(q_{WN}(t)) & 0 \end{pmatrix} \tag{16}$$

where $a_{WNPN}(q_{PN}(t))$ is updated according to the inoperability of PN at time t, whereas $a_{PNWN}(q_{WN}(t))$ is updated based on the inoperability of WN.

Two distinct operability disruption scenarios are considered: medium impact with an external shock resulting in 50 % of PN inoperability, and high impact with 80 % of PN inoperability.

The DIIM assumes a static interdependency matrix (Eq. (17)). To ensure a consistent comparison, $\overline{\overline{A}}$ is conservatively defined using the most probable inoperability ranges of PN and WN. These ranges are derived from the histograms in Figs. 15 and Fig. 18, with the last row ($r_5^{PN} = (0.7, 1]$ and $r_5^{WN} = (0.8, 1]$) used to define the coefficients in $\overline{\overline{A}}$ for PN and WN, respectively. Thus, $\overline{\overline{A}}$ is set as:

$$\overline{\overline{A}} = \begin{pmatrix} 0 & 0.93 \\ 0.99 & 0 \end{pmatrix} \tag{17}$$

Note that the 0.93 coefficient for the dependency *PN→WN* is slightly lower than 0.99 for the dependency *WN→PN* due to differences in CIs topologies. As shown in Fig. 19 (a), PN can reach its highest inoperability range (r_5^{PN}) without necessarily disabling any node in $N_{PN\to WN}^{PN}$, preventing cascading effects in WN. In contrast, WN failures leading to (r_5^{WN}) inevitably involve nodes in $N_{WN\to PN}^{WN}$, causing cascading failures in PN as illustrated in Fig. 19 (b).

Table 1 summarizes the results of estimating the inoperability of WN for the two scenarios. Both the static and the multi-state interdependent CIs approaches provide the same results $\begin{pmatrix} q_{WN} \\ q_{PN} \end{pmatrix} = \begin{pmatrix} 0.74 \\ 0.8 \end{pmatrix}$ in high operability disruption scenarios. However, in medium operability disruption scenarios, the static interdependency matrix overestimates WN inoperability due to its conservative dependency on PN (reflected in the constant a_{WNPN}).

This indicates that whereas both approaches align under high operability disruptions, the traditional static interdependency matrix ($\overline{\overline{A}}$) fails to capture the dynamic interactions between CIs in low and medium-disruption scenarios. In contrast, the multi-state approach updates the interdependency coefficient (a_{WNPN}) based on the actual inoperability value of PN at each time t, better reflecting the evolving interdependencies of CIs. These differences become more pronounced over time as the disruption and recovery process progresses.

To further illustrate this, Fig. 20 shows the inoperability curves for each CI using DIIM (recovery considered). The left column represents the inoperability behavior of the WN, whereas the right column corresponds to the PN. The first row of plots represents the high operability disruption scenario, whereas the second row corresponds to the medium operability disruption scenario.

In all plots, the multi-state DIIM (dotted line) shows a faster reduction in inoperability compared to the traditional DIIM (solid line). This is because the multi-state DIIM updates the interdependency coefficients (a_{WNPN} and a_{PNWN}) based on the current inoperability values of the CIs. Meanwhile, the traditional DIIM uses static coefficients, which do not adjust $\overline{\overline{A}}$ to model decreasing inoperability associated with recovery over time.

For initial inoperability values, both approaches produce identical results in the high-impact scenario, as the multi-state DIIM starts with the same values as the traditional DIIM. However, in the medium impact disruption scenario, the multi-state approach adjusts a_{WNPN} to 0.37 for 50 % inoperability of PN (i.e., PN presents an unmet demand of 50 % and falls in inoperability range r_3^{PN}). The interdependency coefficient a_{PNWN} is also updated to 0.02, given that WN inoperability corresponds to inoperability range r_2^{WN}. By comparison, the Boolean model uses static

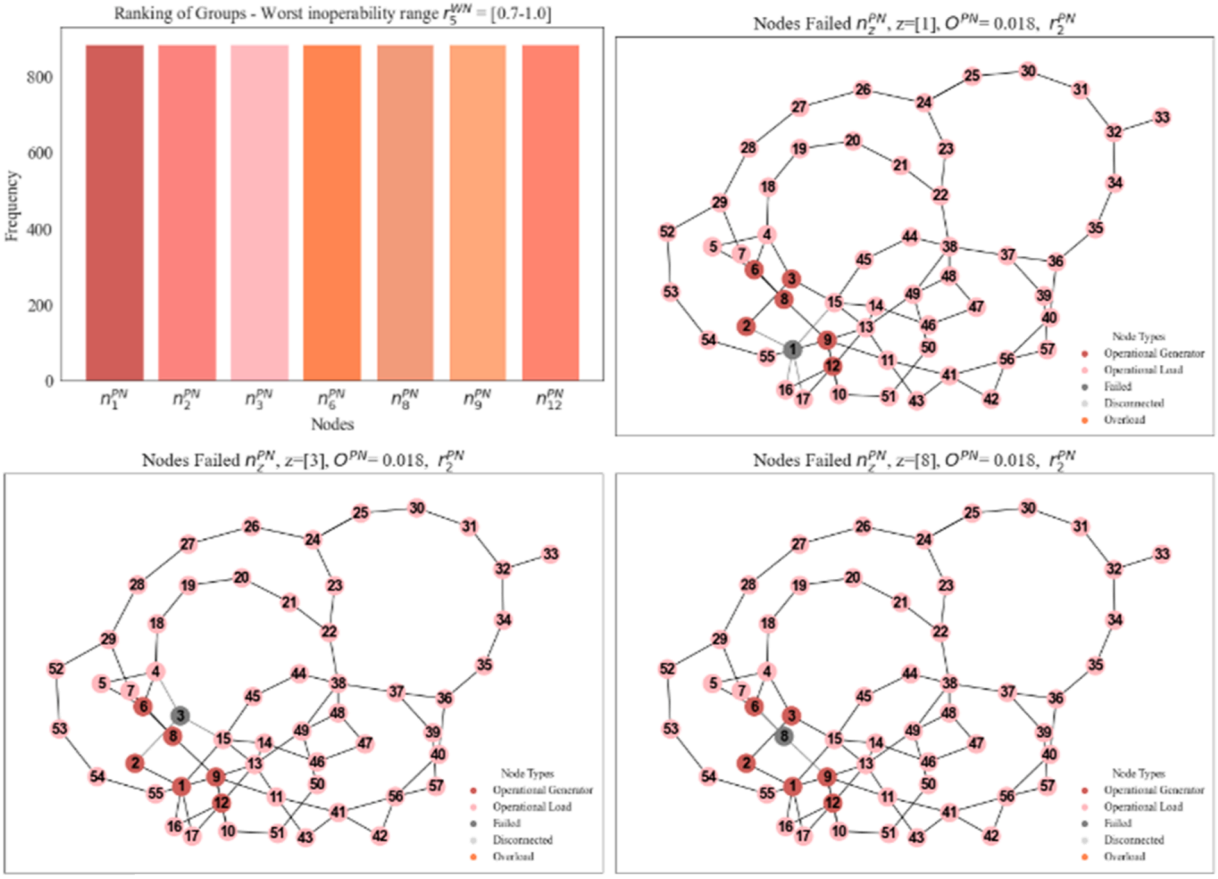

Fig. 22. Dependency ***WN→PN***: analysis of critical nodes in G^{PN}.

values of $a_{WNPN} = 0.93$ and $a_{PNWN} = 0.99$, based on the most likely state condition, which overestimates inoperability.

5.2. Identification of critical nodes in the system of systems

Along with inoperability estimation, the proposed methodology enables the identification of critical nodes, offering insights into the key nodes that most influence cascading failures in the system of systems. By focusing on high impact disruption scenarios, it is possible to find the most relevant nodes for each dependency under study.

Analyzing the *PN→WN* dependency, the most critical nodes in $N_{PN\to WN}^{WN}$ are those more frequently affected by cascading failures from G^{PN}: n_1^{WN}, n_{50}^{WN} and n_{16}^{WN}. Among these, n_1^{WN} is the most critical for WN, as its failure alone can cause complete inoperability of the infrastructure, as shown in Fig. 21. This finding can help effectively plan a resilience-improvement strategy for the interdependent CIs.

Similarly, the analysis of the *WN→PN* dependency in high disruption scenarios shows that all nodes in $N_{WN\to PN}^{PN}$ are equally affected by cascading failures from G^{WN}, as shown in the histogram in Fig. 22. The failure of any single node in $N_{WN\to PN}^{PN}$ results in the same inoperability range of PN (r_2^{PN}) — for example, nodes n_1^{PN}, n_3^{PN} and n_8^{PN} in Fig. 22. This suggests that significant effects on PN occur only when multiple supplier nodes fail simultaneously.

5.3. Adoption of mitigation strategies

Once critical nodes are identified, better informed mitigation strategies can be selected. For example, the owner of the WN might consider equipping the most critical node with a backup power supply, such as an emergency generator at n_1^{WN}, to ensure the continued operation of the water treatment facility (n_1^{WN}) during power outages in PN.

To reflect this retrofitting in the interdependency coefficient a_{WNPN}, the *PN→WN* dependency changes. Specifically, n_1^{WN} is removed from $N_{PN\to WN}^{WN}$ as well as its corresponding power supply nodes in $N_{PN\to WN}^{PN}$, since n_1^{WN} is now independent of PN. The proposed methodology is then applied to this new dependency relation.

Similarly, the owner of PN could invest in a robust water supply system, such as a dedicated backup water reservoir for the highest capacity supplier nodes (n_1^{PN}, n_8^{PN} and n_{12}^{PN}), ensuring their continued operation during disruptions in WN. With this retrofitting, the highest capacity PN supplier nodes become independent of WN. Consequently, they are removed from $N_{WN\to PN}^{PN}$ and their respective water supplier nodes from $N_{WN\to PN}^{WN}$. This modifies the *WN→PN* dependency, requiring a new estimation of interdependency coefficient a_{PNWN}, which is done using the proposed methodology.

Then, assuming the suggested retrofitting for the previously identified critical nodes, the new interdependency coefficients for each inoperability range of PN and WN ($a_{WNPN}[r_k^{PN}]$, $\forall r_k^{PN} \in r^{PN}$ and $a_{PNWN}[r_k^{WN}]$, $\forall r_k^{WN} \in r^{WN}$) are presented in Fig. 23.

To show the effects of CIs retrofitting on the inoperability of the system of systems, two scenarios are simulated using DIIM. The first scenario (left plot in Fig. 24) simulates an initial inoperability of 80 % in PN to show the inoperability behavior of the dependent WN. The second scenario (right plot in Fig. 24) simulates an 80 % initial inoperability in WN. Fig. 24 illustrates the inoperability behavior of WN and PN before and after retrofitting.

The initial inoperability of WN decreases from 0.75 to 0.45, achieving a 30 % reduction in the initial effects, demonstrating the reduced dependency *PN→WN* (left subplot). The initial inoperability of PN reduces from 0.78 to 0.24, achieving a 54 % reduction (right

r^{PN} \ r^{WN}	[0]	(0, 0.2]	(0.2, 0.6]	(0.6, 0.8]	(0.8, 1]	After Retrofitting $a_{WNPN}[r_k^{PN}]$	Before Retrofitting $a_{WNPN}[r_k^{PN}]$
[0]	1 × 0	0 × 0.2	0 × 0.6	0 × 0.8	0 × 1	0	0
(0, 0.3]	0.34 × 0	0.57 × 0.2	0.09 × 0.6	0 × 0.8	0 × 1	0.17	0.18
(0.3, 0.5]	0.11 × 0	0.61 × 0.2	0.28 × 0.6	0 × 0.8	0 × 1	0.29	0.37
(0.5, 0.7]	0 × 0	0.65 × 0.2	0.35 × 0.6	0 × 0.8	0 × 1	0.34	0.60
(0.7, 1]	0 × 0	0.11 × 0.2	0.89 × 0.6	0 × 0.8	0 × 1	0.56	0.94

r^{WN} \ r^{PN}	[0]	(0, 0.3]	(0.3, 0.5]	(0.5, 0.7]	(0.7, 1]	After Retrofitting $a_{PNWN}[r_k^{WN}]$	Before Retrofitting $a_{PNWN}[r_k^{WN}]$
[0]	1 × 0	0 × 0.3	0 × 0.5	0 × 0.7	0 × 1	0	0
(0, 0.2]	1 × 0	0 × 0.3	0 × 0.5	0 × 0.7	0 × 1	0	0.02
(0.2, 0.6]	0.77 × 0	0.23 × 0.3	0 × 0.5	0 × 0.7	0 × 1	0.07	0.09
(0.6, 0.8]	0.04 × 0	0.96 × 0.3	0 × 0.5	0 × 0.7	0 × 1	0.29	0.29
(0.8, 1]	0 × 0	1 × 0.3	0 × 0.5	0 × 0.7	0 × 1	0.3	0.99

Fig. 23. Interdependency coefficients a_{WNPN} and a_{PNWN}, before and after retrofitting in each CI.

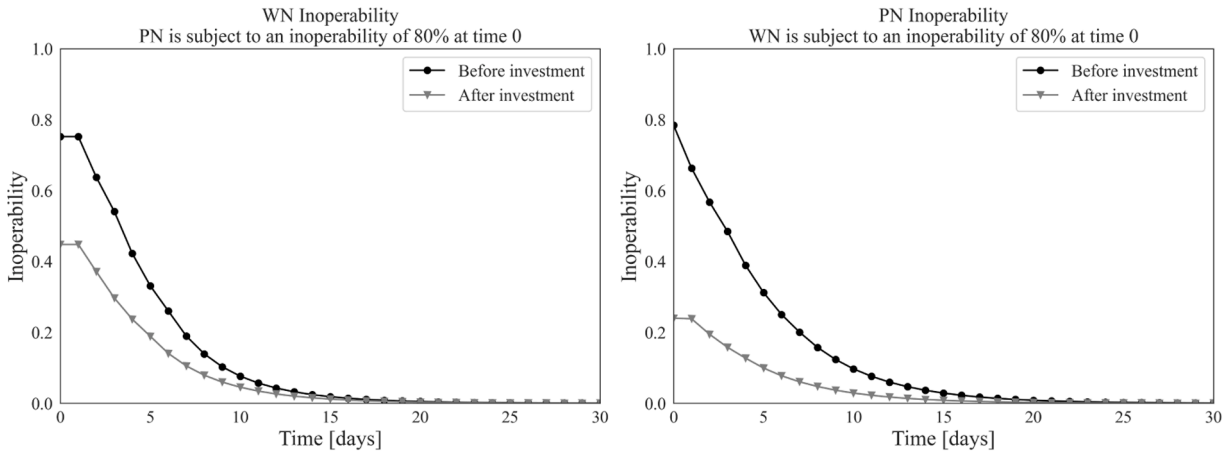

Fig. 24. Inoperability comparison before and after investments in PN and WN.

subplot).

These results demonstrate that targeted resilience-guided investments and retrofitting significantly enhance the resilience of both CIs, leading to substantial reductions in inoperability.

Alternatively, to mitigate inoperability following operational disruptions, enhancing the recovery by reducing the recovery time can also serve the scope of a resilience-guided CI retrofitting [50]. Fig. 25 compares the results when the matrix $\overline{\overline{K}}$ assumes 14 days of recovery for WN and 21 days for PN (continuous dark line) with those of a recovery time decreased (continuous light line) by 30 %, from 14 to 10 days for WN and from 21 to 15 days for PN.

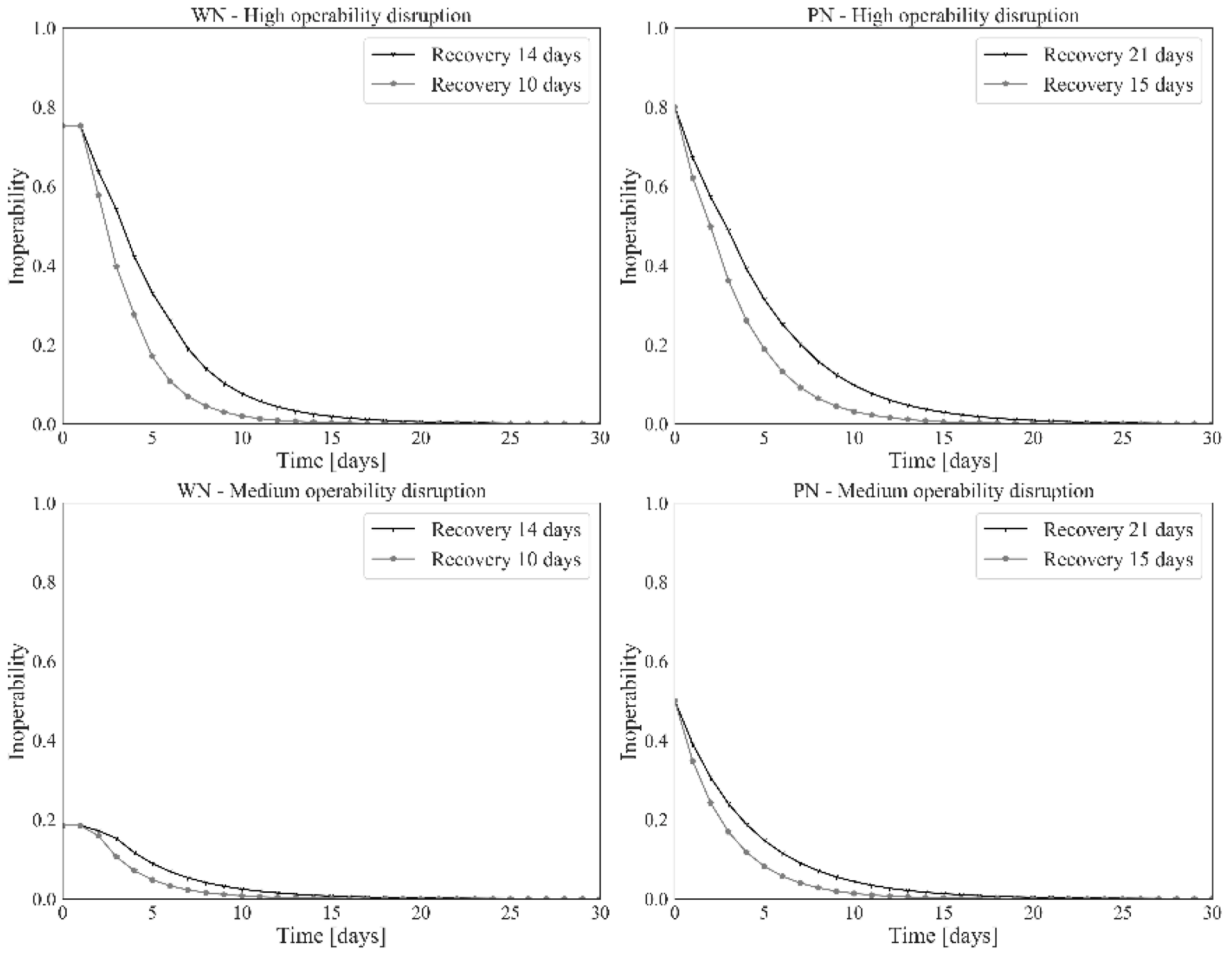

Fig. 25. Impact of 30 % reduction in recovery times on inoperability curves for WN and PN under high and medium operability disruptions.

6. Conclusions

This paper introduces a novel approach for modeling interdependencies between multi-state interdependent CIs in a system of systems. By considering the dynamic nature of disruption cascades in multi-state interdependent CIs, the proposed approach accounts for varying degrees of operability and inoperability between the multi-state CIs.

The approach unfolds in three phases: (i) delineating the structure and operational characteristics of each CI using network theory, (ii) mapping the interdependencies between CIs based on the combination of subsystems/components' inoperability states in individual CIs that lead the dependent CIs to a specific state of inoperability upon disruption and, (iii) estimating the interdependency coefficients of the DIIM by simulation. The approach involves a stochastic exploration of scenarios to mine out multi-state interdependent CIs. Unlike traditional DIIM, this structured procedure reduces the expert judgment and the subjectivity of the results when updating the interdependency coefficients, reflecting the current inoperability state of CIs.

A case study has been presented concerning a system of systems of a power network and a water network, each one with five possible inoperability ranges. A comparative analysis with the traditional DIIM approach shows the benefits of the multi-state methodology. In addition, the proposed methodology allows for an in-depth analysis of the internal state of CIs, providing relevant information to owner and managers. This includes the identification of critical nodes in the interdependency relation with other CIs and the effects of investing in the robustness of these nodes. Thus, the traditional DIIM (holistic approach), which provides valuable insights for planners of system of systems, is complemented with network theory (reductionist approach) and this combination delivers relevant operational information to the operators of the infrastructures.

It is interesting to observe that the values of the interdependency coefficients in our case study, especially for the highest inoperability ranges of CIs (r_5^{PN} for PN and r_5^{WN} for WN), are significantly larger than those reported in other DIIM applications (e.g., [18,21,28]). This difference arises because previous studies make use of a single lumped interdependency coefficient, which averages best- and worst-case scenarios, shadowing the differences among the coefficients of the (realistically) different multi-states of inoperability.

Specifically, our findings highlight that Eq. (4) is sensible to high interdependency coefficients in $\overline{\overline{A}}$: when one CI is heavily dependent on another impacted CI, the inoperability reduction is prolonged as the interdependency effects are compounded over time, making individual recovery efforts insufficient without significant recovery of the dependent CI.

As future research, while the proposed approach efficiently estimates interdependency coefficients, further advancements in scenario generation could enhance computational efficiency even more. The authors aim to develop advanced Monte Carlo simulation and artificial intelligence approaches for generating, exploring and analyzing operational disruption scenarios in complex CIs, where the number of possible combinations of the states of the nodes between interdependent multi-state CIs become large. Also, the recovery matrix level will be further analyzed for a more comprehensive representation of the actual management of multi-state elements of CIs.

CRediT authorship contribution statement

Maria Valentina Clavijo Mesa: Writing – original draft, Software, Methodology, Conceptualization. **Francesco Di Maio:** Writing – review & editing, Supervision, Methodology, Funding acquisition, Conceptualization. **Enrico Zio:** Writing – review & editing, Supervision, Funding acquisition, Conceptualization.

Declaration of competing interest

The authors declare that they have no known competing financial interests or personal relationships that could have appeared to influence the work reported in this paper.

Acknowledgements

This work was supported by the Italian National Recovery and Resilience programme (PNRR -Piano Nazionale di Ripresa e Resilienza).

Appendix A. Operational disruption propagation in a generic k CI

This appendix details the propagation of operational disruption within a generic k CI, where nodes N^k are classified as either supplier nodes N_S^k or demand nodes N_D^k, thus $N^k = N_S^k \bigcup N_D^k$.

The states of generic z demand node $n_z^k \in N_D^k$, and generic u supplier node $n_u^k \in N_S^k$, along with the states of the edges connecting these nodes, are exposed in Table A.1.

Table A.1
Node and edge states of the generic k CI.

Entity	State description
Generic demand node $n_z^k \in N_D^k$	Perfect functioning ($x_1^{n_z^k}$)
	Disconnected ($x_2^{n_z^k}$)
	Inoperable ($x_3^{n_z^k}$)
Generic supplier node $n_u^k \in N_S^k$	Perfect functioning ($x_1^{n_u^k}$)
	Disconnected ($x_2^{n_u^k}$)
	Overload ($x_3^{n_u^k}$)
	Inoperable ($x_4^{n_u^k}$)
Generic edge $e_{op}^{(k,k)} \in E^{(k,k)}$ $e_{op}^{(k,k)} = \left(n_o^k, n_p^k\right) \subseteq N^k \times N^k$	Available ($x_1^{e_{op}^{(k,k)}}$)
	Unavailable ($x_2^{e_{op}^{(k,k)}}$)

Each $n_z^k \in N_D^k$ has a nominal demand $\widehat{d}^{n_z^k}$, and each supplier node $n_u^k \in N_S^k$ has an initial load $\widehat{l}^{n_u^k}$ and a maximum load capacity $c^{n_u^k}$.

When all nodes of the k CI are in the perfect functioning state $x_1^{n_z^k} = 1\ \forall n_z^k \in N^k$, the k CI itself is in perfect functioning state (X_1^k). The demand met in this state is denoted by $D(X_1^k)$, and can be estimated as:

$$D(X_1^k) = \sum_{n_z^k \in N_D^k} \widehat{d}^{n_z^k} \tag{18}$$

Upon the occurrence of an operational disruption scenario s, the state of the nodes N^k undergoes changes, thereby altering the state of the infrastructure to X_s^k. The met demand in this scenario, denoted as $D(X_s^k)$, can be estimated by accounting for reductions due to various effects on the infrastructure:

$$D(X_s^k) = D(X_1^k) - \widetilde{D}(X_s^k)_r - \widetilde{D}(X_s^k)_d - \widetilde{D}(X_s^k)_o \tag{19}$$

Where $\widetilde{D}(X_s^k)_r$ represents the unmet demand due to nodes becoming inoperable as direct effects of the disruption, $\widetilde{D}(X_s^k)_d$ is the demand unmet due to disconnections, and $\widetilde{D}(X_s^k)_o$ denotes the unmet demand resulting from overload supplier nodes.

To estimate $\widetilde{D}(X_s^k)_r$, nodes directly impacted by the disruption are assumed to be in an inoperable state, and the demand from these nodes is summed as follows:

$$\widetilde{D}(X_s^k)_r = \sum \widehat{d}^{n_z^k}\ \forall\left(n_z^k \in N_D^k \middle| x_3^{n_z^k} = 1\right) \tag{20}$$

Furthermore, the edges from nodes directly affected are marked as unavailable:

$$x_2^{e_{op}^{(k,k)}} = 1,\ \forall\left(n_o^k \in N^k \middle| x_3^{n_o^k} = 1\right) \tag{21}$$

This unavailability affects the topology of the network, leading to loss of certain connections [51,52]. To estimate $\widetilde{D}(X_s^k)_d$ we follow the approach proposed by [46,53], which involves identifying the largest connected subgraph $\widetilde{G}_s^k$ under scenario s. Nodes and edges not included in $\widetilde{G}_s^k$ are updated to a disconnected state:

$$x_2^{n_z^k} = 1, \quad \forall n_z^k \notin \widetilde{G}_s^k$$
$$x_2^{e_{zp}^{(k,k)}} = 1, \quad \forall \left(n_z^k \middle| x_2^{n_z^k} = 1 \right) \tag{22}$$

$\widetilde{D}(X_s^k)_d$ is the total demand of all demand nodes in a disconnected state, computed as:

$$\widetilde{D}(X_s^k)_d = \sum \widehat{d}^{n_z^k} \ \forall \left(n_z^k \in N_D^k \middle| x_2^{n_z^k} = 1 \right) \tag{23}$$

The impact of overload supplier nodes necessitates assessing the capacity of operational supplier nodes within $\widetilde{G}_s^k$, denoted as $C(\widetilde{G}_s^k)$, and the demand requirements within the cluster, denoted as $D(\widetilde{G}_s^k)$. These metrics are estimated based on the operational supplier and demand nodes within the cluster, as follows:

$$C(\widetilde{G}_s^k) = \sum c^{n_u^k} \ \forall \left(n_u^k \in N_S^k \cap \ \widetilde{G}_s^k \middle| x_1^{n_u^k} = 1 \right) \tag{24}$$

$$D(\widetilde{G}_s^k) = \sum \widehat{d}^{n_z^k} \ \forall \left(n_z^k \in N_D^k \cap \ \widetilde{G}_s^k \middle| x_1^{n_z^k} = 1 \right) \tag{25}$$

Based on the calculated capacity $C(\widetilde{G}_s^k)$ and demand $D(\widetilde{G}_s^k)$ within the cluster, a redistribution of load among the operational supplier nodes is executed. This redistribution prioritizes supplier nodes with greater capacities to handle increased demands, in alignment with the methodology proposed by [53]. The estimated final load for each operational supplier node n_u^k, denoted as $\widetilde{l}^{n_u^k}$ is calculated as:

$$\widetilde{l}^{n_u^k} = \widehat{l}^{n_u^k} + \left[D(\widetilde{G}_s^k) \times \frac{c^{n_u^k}}{C(\widetilde{G}_s^k)} \right] \tag{26}$$

Should the final load $\widetilde{l}^{n_u^k}$ of a supplier node n_u^k exceeds its capacity, the node's state transitions from operational ($x_1^{n_u^k}$) to overload ($x_3^{n_u^k}$). In such cases, the node's final load is adjusted to its maximum capacity:

$$\widetilde{l}^{n_u^k} = c^{n_u^k} \ \forall \left(n_u^k \in N_S^k \cap \ \widetilde{G}_s^k \middle| \widetilde{l}^{n_u^k} > c^{n_u^k} \right) \tag{27}$$

To determine $\widetilde{D}(X_s^k)_o$, the total load across the cluster $L(\widetilde{G}_s^k)$ is assessed, calculated as the sum of the final loads of operational supplier nodes not in an inoperable state:

$$L(\widetilde{G}_s^k) = \sum \widetilde{l}^{n_u^k} \ \forall \left(n_u^k \in N_S^k \cap \ \widetilde{G}_s^k \middle| x_4^{n_u^k} \neq 1 \right) \tag{28}$$

$\widetilde{D}(X_s^k)_o$ quantifies the lost demand given overload, representing the difference between the required demand in the cluster compared and the effective load supported by the operational supplier nodes:

$$\widetilde{D}(X_s^k)_o = D(\widetilde{G}_s^k) - L(\widetilde{G}_s^k) \tag{29}$$

This difference, $\widetilde{D}(X_s^k)_o$, is zero if the operational load suffices to meet the cluster's demand. However, should supplier nodes enter an overload state, a discrepancy emerges between the required and available capacities.

Given the final state of all nodes, the overall met demand $D(X_s^k)$ can be estimated. Table A.2 presents a pseudocode summarizing this process.

Table A.2
Pseudocode of operability disruption propagation in a generic k CI.

Inputs for operability disruption in a generic *k* CI:
Nodes in the *k*-th CI, N^k
Supplier nodes in the *k*-th CI, N_S^k
Demand nodes in the *k*-th CI, N_D^k
Demand of demand nodes in the *k*-th CI, $\widehat{d}^{n_z^k} \ \forall n_z^k \in N_D^k$
Initial load of supplier nodes in the *k*-th CI, $\widehat{l}^{n_u^k} \ \forall n_u^k \in N_S^k$
Capacity of supplier nodes in the *k*-th CI, $c^{n_u^k} \ \forall n_u^k \in N_S^k$
Initial state conditions for scenario *s*, $X_{s^o}^k$
Demand met by the *k*-th CI in perfect state, $D(X_1^k)$
for each node $\left(n_z^k \in N_D^k \middle| x_3^{n_z^k} = 1 \right)$:
set $\widetilde{D}\left(X_{s^o}^k\right)_r = \widetilde{D}\left(X_{s^o}^k\right)_r + \widehat{d}^{n_z^k}$ unmet demand given demand node's remotion
update $x_2^{e_{zp}^{(k,k)}} = 1$ to deactivate the edges of removed demand nodes
end
for each node $\left(n_u^k \in N_S^k \middle| x_4^{n_u^k} = 1 \right)$:
update $x_2^{e_{up}^{(k,k)}} = 1$ to deactivate the edges of removed supplier nodes
end
define $\widetilde{G}_{s^o}^k$ as the largest connected cluster under initial conditions of scenario s^o in the *k* CI

(*continued on next page*)

Table A.2 (*continued*)

Inputs for operability disruption in a generic k CI:	
9	**for each** node $n_z^k \notin \widetilde{G}_{s^o}^k$ and $x_1^{n_z^k} = 1$:
10	**set** $\widetilde{D}\left(X_{S^o}^k\right)_d = \widetilde{D}\left(X_{S^o}^k\right)_d + \widehat{d}^{n_z^k}$ unmet demand given demand node's disconnection
11	**update** $x_2^{n_z^k} = 1$ to activate disconnection state for those nodes
12	**end**
13	**set** $D(\widetilde{G}_{s^o}^k)$ required demand in the largest connected cluster
14	**set** $C(\widetilde{G}_{s^o}^k)$ supplier capacity in the largest connected cluster
15	**for each** node $n_u^k \in N_S^k$ and $\widetilde{G}_{s^o}^k$
16	**set** $\widetilde{l}^{n_u^k}$ final load of supplier nodes
17	**if** $\widetilde{l}^{n_u^k} > c^{n_u^k}$:
18	**set** $\widetilde{l}^{n_u^k} = c^{n_u^k}$ final load of node as its maximum capacity
19	**set** $L(\widetilde{G}_{s^o}^k) = L(\widetilde{G}_{s^o}^k) + \widetilde{l}^{n_u^k}$ supplier capacity in the largest connected cluster
20	**else:**
21	**set** $L(\widetilde{G}_{s^o}^k) = L(\widetilde{G}_{s^o}^k) + \widetilde{l}^{n_u^k}$ supplier capacity in the largest connected cluster
22	**end**
23	**end**
24	**set** $\widetilde{D}\left(X_{S^o}^k\right)_o = D(\widetilde{G}_{s^o}^k) - L(\widetilde{G}_{s^o}^k)$ unmet demand given supplier node's overload
25	**set** final state of the k CI under scenario s, X_{sf}^k
26	**set** $D(X_{sf}^k) = D(X_1^k) - \widetilde{D}\left(X_{S^o}^k\right) - \widetilde{D}\left(X_{S^o}^k\right)_d - \widetilde{D}\left(X_{S^o}^k\right)_o$
27	**store** $D(X_{sf}^k)$ and X_{sf}^k
Output: $D(X_{sf}^k)$ and X_{sf}^k, the attended demand of the k CI and the final state of the infrastructure under scenario s, respectively	

Appendix B. Characterization of nodes in G^{PN} and G^{WN}

The demand for each node in G^{PN} and G^{WN} is based on the initial bus demands reported in the IEEE datasets for the IEEE57-bus test system and the IEEE85-bus system, respectively [54,55]. This data is detailed for each demand node in Table Table B.1. For the supplier nodes, both the initial load and capacity are derived from these datasets, with the capacity corresponding to the maximum reported output. This information is summarized in Table B.2.

Table B.1
Demand for demand nodes in G^{PN} and G^{WN}.

Demand of nodes in G^{PN} [MW]							
Node	Demand	Node	Demand	Node	Demand	Node	Demand
n_4^{PN}	0	n_{21}^{PN}	0	n_{34}^{PN}	0	n_{46}^{PN}	0
n_5^{PN}	13	n_{22}^{PN}	0	n_{35}^{PN}	6	n_{47}^{PN}	29.7
n_7^{PN}	0	n_{23}^{PN}	6.3	n_{36}^{PN}	6	n_{48}^{PN}	0
n_{10}^{PN}	5	n_{24}^{PN}	0	n_{37}^{PN}	0	n_{49}^{PN}	18
n_{11}^{PN}	0	n_{25}^{PN}	6.3	n_{38}^{PN}	14	n_{50}^{PN}	21
n_{13}^{PN}	18	n_{26}^{PN}	0	n_{39}^{PN}	0	n_{51}^{PN}	20
n_{14}^{PN}	10.5	n_{27}^{PN}	9.3	n_{40}^{PN}	0	n_{52}^{PN}	4.9
n_{15}^{PN}	22	n_{28}^{PN}	4.6	n_{41}^{PN}	6.3	n_{53}^{PN}	20
n_{16}^{PN}	43	n_{29}^{PN}	17	n_{42}^{PN}	7.1	n_{54}^{PN}	4.1
n_{17}^{PN}	42	n_{30}^{PN}	3.6	n_{43}^{PN}	2	n_{55}^{PN}	6.8
n_{18}^{PN}	27.2	n_{31}^{PN}	5.8	n_{44}^{PN}	12	n_{56}^{PN}	7.6
n_{19}^{PN}	3.3	n_{32}^{PN}	1.6	n_{45}^{PN}	0	n_{57}^{PN}	6.7
n_{20}^{PN}	2.3	n_{33}^{PN}	3.8				
Demand of nodes in G^{WN} $\left[\frac{m^3}{h}\right]$							
Node	Demand	Node	Demand	Node	Demand	Node	Demand
n_2^{WN}	0	n_{23}^{WN}	56	n_{44}^{WN}	35.28	n_{65}^{WN}	0
n_3^{WN}	0	n_{24}^{WN}	35.28	n_{45}^{WN}	35.28	n_{66}^{WN}	56
n_4^{WN}	56	n_{25}^{WN}	35.28	n_{46}^{WN}	35.28	n_{67}^{WN}	0
n_5^{WN}	0	n_{26}^{WN}	56	n_{47}^{WN}	14	n_{68}^{WN}	0
n_6^{WN}	35.28	n_{27}^{WN}	0	n_{48}^{WN}	0	n_{69}^{WN}	56
n_7^{WN}	0	n_{28}^{WN}	56	n_{49}^{WN}	0	n_{70}^{WN}	0
n_8^{WN}	35.28	n_{29}^{WN}	0	n_{50}^{WN}	36.28	n_{71}^{WN}	35.28
n_9^{WN}	0	n_{30}^{WN}	35.28	n_{51}^{WN}	56	n_{72}^{WN}	56
n_{10}^{WN}	0	n_{31}^{WN}	35.28	n_{52}^{WN}	0	n_{73}^{WN}	0
n_{11}^{WN}	56	n_{32}^{WN}	0	n_{53}^{WN}	35.28	n_{74}^{WN}	56
n_{12}^{WN}	0	n_{33}^{WN}	14	n_{54}^{WN}	56	n_{75}^{WN}	35.28
n_{13}^{WN}	0	n_{34}^{WN}	0	n_{55}^{WN}	56	n_{76}^{WN}	56

(*continued on next page*)

Table B.1 (*continued*)

Demand of nodes in G^{PN} [MW]							
Node	Demand	Node	Demand	Node	Demand	Node	Demand
n_{14}^{WN}	35.28	n_{35}^{WN}	0	n_{56}^{WN}	14	n_{77}^{WN}	14
n_{15}^{WN}	35.28	n_{36}^{WN}	35.28	n_{57}^{WN}	56	n_{78}^{WN}	56
n_{16}^{WN}	35.28	n_{37}^{WN}	56	n_{58}^{WN}	0	n_{79}^{WN}	35.28
n_{17}^{WN}	112	n_{38}^{WN}	56	n_{59}^{WN}	56	n_{80}^{WN}	56
n_{18}^{WN}	56	n_{39}^{WN}	56	n_{60}^{WN}	0	n_{81}^{WN}	0
n_{19}^{WN}	56	n_{40}^{WN}	35.28	n_{61}^{WN}	56	n_{82}^{WN}	56
n_{20}^{WN}	35.28	n_{41}^{WN}	0	n_{62}^{WN}	56	n_{83}^{WN}	35.28
n_{21}^{WN}	35.28	n_{42}^{WN}	35.28	n_{63}^{WN}	14	n_{84}^{WN}	14
n_{22}^{WN}	35.28	n_{43}^{WN}	35.28	n_{64}^{WN}	0	n_{85}^{WN}	35.28

Table B.2
Initial load and capacity for supplier nodes in $\boldsymbol{G^{PN}}$ and $\boldsymbol{G^{WN}}$.

Supplier nodes in G^{PN}			Supplier nodes in G^{WN}		
Node	Initial load [MW]	Capacity [MW]	Node	Initial load $\left[\frac{m^3}{h}\right]$	Capacity $\left[\frac{m^3}{h}\right]$
n_1^{PN}	0	575.88	n_1^{WN}	2514.28	2639.99
n_2^{PN}	0	100			
n_3^{PN}	21.4	140			
n_6^{PN}	0	100			
n_8^{PN}	241.2	550			
n_9^{PN}	0	100			
n_{12}^{PN}	166.2	410			

Data availability

Data will be made available on request.

References

[1] Wells EM, Boden M, Tseytlin I, Linkov I. Modeling critical infrastructure resilience under compounding threats: a systematic literature review. Progress Disaster Sci. 2022;15:100244. https://doi.org/10.1016/j.pdisas.2022.100244.

[2] Huang CN, Liou JJH, Chuang YC. A method for exploring the interdependencies and importance of critical infrastructures. Knowl Based Syst 2014;55:66–74. https://doi.org/10.1016/j.knosys.2013.10.010.

[3] Pant R, Barker K, Zobel CW. Static and dynamic metrics of economic resilience for interdependent infrastructure and industry sectors. Reliab Eng Syst Saf 2014;125:92–102. https://doi.org/10.1016/j.ress.2013.09.007.

[4] Kujawski E. Multi-period model for disruptive events in interdependent systems. Syst Eng 2006;9:281–95. https://doi.org/10.1002/sys.20057.

[5] Mendelssohn IA, Andersen GL, Baltz DM, Caffey RH, Carman KR, Fleeger JW, et al. Oil impacts on coastal wetlands: implications for the mississippi river delta ecosystem after the deepwater horizon oil spill. Bioscience 2012;62:562–74. https://doi.org/10.1525/bio.2012.62.6.7.

[6] Fan C, Mostafavi A. A graph-based method for social sensing of infrastructure disruptions in disasters. Comput-Aided Civ Infrastruct Eng 2019;34:1055–70. https://doi.org/10.1111/mice.12457.

[7] Ouyang M. Review on modeling and simulation of interdependent critical infrastructure systems. Reliab Eng Syst Saf 2014;121:43–60. https://doi.org/10.1016/j.ress.2013.06.040.

[8] Johansson J, Hassel H. An approach for modelling interdependent infrastructures in the context of vulnerability analysis. Reliab Eng Syst Saf 2010;95:1335–44. https://doi.org/10.1016/j.ress.2010.06.010.

[9] Chang SE, McDaniels T, Fox J, Dhariwal R, Longstaff H. Toward disaster-resilient cities: characterizing resilience of infrastructure systems with expert judgments. Risk Anal 2014;34:416–34. https://doi.org/10.1111/risa.12133.

[10] Bakhtiari S, Najafi MR, Goda K, Peerhossaini H. A dynamic Bayesian network approach to characterize multi-hazard risks and resilience in interconnected critical infrastructures. Reliab Eng Syst Saf 2025;257:110815. https://doi.org/10.1016/j.ress.2025.110815.

[11] Cheng Q, Xie L, Wang Z, Liu Z, Lu X, Wang X. Multilevel assessment method for post-earthquake functionality of medical buildings considering component–department–floor interdependencies. Reliab Eng Syst Saf 2024;251:110379. https://doi.org/10.1016/j.ress.2024.110379.

[12] Sharma N, Gardoni P. Mathematical modeling of interdependent infrastructure: an object-oriented approach for generalized network-system analysis. Reliab Eng Syst Saf 2022;217:108042. https://doi.org/10.1016/j.ress.2021.108042.

[13] Sharma N, Tabandeh A, Gardoni P. Regional resilience analysis: A multiscale approach to optimize the resilience of interdependent infrastructure. Comput-Aided Civ Infrastruct Eng 2020;35:1315–30. https://doi.org/10.1111/mice.12606.

[14] Gong S, Chen L, Zhou Q, Gao X, Shen F. Vulnerability evolution of critical infrastructures: a multidimensional environment-integrated system dynamics analysis. Reliab Eng Syst Saf 2025;256:110719. https://doi.org/10.1016/j.ress.2024.110719.

[15] Zhou S, Ng ST, Yang Y, Xu JF. Delineating infrastructure failure interdependencies and associated stakeholders through news mining: the case of Hong Kong's water pipe bursts. J Manage Eng 2020;36. https://doi.org/10.1061/(ASCE)ME.1943-5479.0000821.

[16] Sun W, Bocchini P, Davison BD. Overview of interdependency models of critical infrastructure for resilience assessment. Nat Hazards Rev 2022;23. https://doi.org/10.1061/(asce)nh.1527-6996.0000535.

[17] Setola R, Rosato V, Kyriakides E, Rome E. Managing the complexity of critical infrastructures: A modelling and simulation approach. 2016.

[18] Jonkeren O, Giannopoulos G. Analysing critical infrastructure failure with a resilience inoperability input-output model. Econ Syst Res 2014;26:39–59. https://doi.org/10.1080/09535314.2013.872604.

[19] Haimes YY, Jiang P. Leontief-based model of risk in complex interconnected infrastructures. J Infrastruct Syst 2001;7:1–12.

[20] Setola R, De Porcellinis S, Sforna M. Critical infrastructure dependency assessment using the input-output inoperability model. Int J Crit Infrastruct Prot 2009;2:170–8. https://doi.org/10.1016/j.ijcip.2009.09.002.

[21] Jin J, Zhou H. A demand-side inoperability input–Output Model for strategic risk management: insight from the COVID-19 outbreak in Shanghai, China. Sustainability 2023;15:4003. https://doi.org/10.3390/su15054003.

[22] Santos J, Roquel KIDZ, Lamberte A, Tan RR, Aviso KB, Tapia JFD, et al. Assessing the economic ripple effects of critical infrastructure failures using the dynamic inoperability input-output model: a case study of the Taal Volcano eruption. Sustain Resilient Infrast. 2023;8:68–84. https://doi.org/10.1080/23789689.2022.2127999.

[23] Oosterhaven J. On the limited usability of the inoperability IO model*. Econ Syst Res 2017;29:452–61. https://doi.org/10.1080/09535314.2017.1301395.

[24] Barker K, Rocco SCM. Evaluating uncertainty in risk-based interdependency modeling with interval arithmetic. Econ Syst Res 2011;23:213–32. https://doi.org/10.1080/09535314.2011.572064.

[25] Setola R, Oliva G, Conte F. Time-varying input-output inoperability model. J Infrastruct Syst 2013;19:47–57. https://doi.org/10.1061/(asce)is.1943-555x.0000099.

[26] Barker K, Haimes YY. Assessing uncertainty in extreme events: applications to risk-based decision making in interdependent infrastructure sectors. Reliab Eng Syst Saf 2009;94:819–29. https://doi.org/10.1016/j.ress.2008.09.008.
[27] Galbusera L, Azzini I, Jonkeren O, Giannopoulos G. Inoperability input-output modeling: inventory optimization and resilience estimation during critical events. ASCE ASME J Risk Uncertain Eng Syst A Civ Eng 2016;2. https://doi.org/10.1061/AJRUA6.0000861.
[28] Lian C, Halmes YY. Managing the risk of terrorism to interdependent infrastructure systems through the Dynamic inoperability input-Output model. Syst Eng 2006;9:241–58. https://doi.org/10.1002/sys.20051.
[29] Santos JR, Yu KDS, Pagsuyoin SAT, Tan RR. Time-varying disaster recovery model for interdependent economic systems using hybrid input-output and event tree analysis. Econ Syst Res 2014;26:60–80. https://doi.org/10.1080/09535314.2013.872602.
[30] Ramos Carvajal M del C, Blanc Díaz M. The foundations of dynamic input-output revisited: ¿Does dynamic input-output belong to growth theory? Https://DialnetUnIriojaEs/Servlet/Extart?Codigo=1252455 2002.
[31] Wang Y, Gao S, Wang F. Measurement of power grid resilience based on a dynamic inoperability input–Output model. Front Phys 2022;10. https://doi.org/10.3389/fphy.2022.895267.
[32] He X, Cha EJ. Modeling the damage and recovery of interdependent critical infrastructure systems from natural hazards. Reliab Eng Syst Saf 2018;177:162–75. https://doi.org/10.1016/j.ress.2018.04.029.
[33] Xu W, Wang Z, Hong L, He L, Chen X. The uncertainty recovery analysis for interdependent infrastructure systems using the dynamic inoperability input-output model. Int J Syst Sci 2015;46:1299–306. https://doi.org/10.1080/00207721.2013.822121.
[34] Johansson J, Hassel H, Zio E. Reliability and vulnerability analyses of critical infrastructures: comparing two approaches in the context of power systems. Reliab Eng Syst Saf 2013;120:27–38. https://doi.org/10.1016/j.ress.2013.02.027.
[35] Mühlhofer E, Koks EE, Kropf CM, Sansavini G, Bresch DN. A generalized natural hazard risk modelling framework for infrastructure failure cascades. Reliab Eng Syst Saf 2023;234:109194. https://doi.org/10.1016/j.ress.2023.109194.
[36] Kelly S. Estimating economic loss from cascading infrastructure failure: a perspective on modelling interdependency. Infrastruct Compl 2015;2:7. https://doi.org/10.1186/s40551-015-0010-y.
[37] Salomon J, Broggi M, Kruse S, Weber S, Beer M. Resilience decision-making for complex systems. ASCE-ASME J Risk Uncertainty Eng Syst, Part B: Mech Eng 2020;6. https://doi.org/10.1115/1.4044907.
[38] Zhang C, Wang Y, Zheng T, Wang C, Zhang K. Identifying critical weak points of power-gas integrated energy system based on complex network theory. Reliab Eng Syst Saf 2024;246:110054. https://doi.org/10.1016/j.ress.2024.110054.
[39] Bompard E, Pons E, Wu Di. Extended topological metrics for the analysis of power grid vulnerability. IEEE Syst J 2012;6:481–7. https://doi.org/10.1109/JSYST.2012.2190688.
[40] Salomon J, Behrensdorf J, Winnewisser N, Broggi M, Beer M. Multidimensional resilience decision-making for complex and substructured systems. Resilient Cities Struct. 2022;1:61–78. https://doi.org/10.1016/j.rcns.2022.10.005.
[41] Wang K, Xu Z, Liu Y, Fang Y. Resilience enhancement for multistate interdependent infrastructure networks: from a preparedness perspective. IEEE Trans Reliab 2023;72:190–203. https://doi.org/10.1109/TR.2021.3132774.
[42] Rinaldi SM, Peerenboom JP, Kelly TK. Identifying, understanding, and analyzing critical infrastructure interdependencies. IEEE Control Syst 2001;21:11–25. https://doi.org/10.1109/37.969131.
[43] Kroger Wolfgang, Zio Enrico. Chapter 2: Properties of critical infrastructures. Vulnerable Systems; 2011. p. 9–30.
[44] Wang Y, Guo P, Wu Y, Chen Y, Zio E. Vulnerability assessment of interdependent infrastructures based on a cascading failure model. In: 2022 6th International Conference on System Reliability and Safety (ICSRS). IEEE; 2022. p. 40–4. https://doi.org/10.1109/ICSRS56243.2022.10067571.
[45] Zio Enrico, Sansavini Giovanni. Modeling failure cascades in critical infrastructures with physically-characterized components and interdependencies. In: ESREL 2010 Annual Conference; 2010. p. 652–61.
[46] Wu Y, Guo P, Wang Y, Du M, Wang X, Zhang D. Vulnerability analysis of interdependent infrastructures considering the sensitivity of components to different risks. In: 2023 IEEE International Conference on Systems, Man, and Cybernetics (SMC). IEEE; 2023. p. 2403–8. https://doi.org/10.1109/SMC53992.2023.10394131.
[47] Popov I. Multi-supplier power grid framework based on multicommodity routing. In: 2015 International Energy and Sustainability Conference (IESC). IEEE; 2015. p. 1–7. https://doi.org/10.1109/IESC.2015.7384387.
[48] Rubido N, Grebogi C, Baptista MS. Resiliently evolving supply-demand networks. Phys Rev E 2014;89:012801. https://doi.org/10.1103/PhysRevE.89.012801.
[49] Almoghathawi Y, Barker K, Albert LA. Resilience-driven restoration model for interdependent infrastructure networks. Reliab Eng Syst Saf 2019;185:12–23. https://doi.org/10.1016/j.ress.2018.12.006.
[50] Johansen C, Tien I. Probabilistic multi-scale modeling of interdependencies between critical infrastructure systems for resilience. Sustain Resilient Infrast. 2018;3:1–15. https://doi.org/10.1080/23789689.2017.1345253.
[51] Li D, Zhang Q, Zio E, Havlin S, Kang R. Network reliability analysis based on percolation theory. Reliab Eng Syst Saf 2015;142:556–62. https://doi.org/10.1016/j.ress.2015.05.021.
[52] Zhang D, Du F, Huang H, Zhang F, Ayyub BM, Beer M. Resiliency assessment of urban rail transit networks: Shanghai metro as an example. Saf Sci 2018;106:230–43. https://doi.org/10.1016/j.ssci.2018.03.023.
[53] Wang S, Lv W, Zhao L, Nie S, Stanley HE. Structural and functional robustness of networked critical infrastructure systems under different failure scenarios. Physica A 2019;523:476–87. https://doi.org/10.1016/j.physa.2019.01.134.
[54] MATPOWER. Case 57 Power flow data for IEEE 57 bus test case. Https://MatpowerOrg/Docs/Ref/Matpower50/Case57Html 2014.
[55] Medina-Quesada Á, Montoya OD, Hernández JC. Derivative-free power flow solution for bipolar DC networks with multiple constant power terminals. Sensors 2022;22:2914. https://doi.org/10.3390/s22082914.